



Study on nonlinear dynamics of rigid-flexible coupling multi-link mechanism considering various kinds of clearances

Linjing Xiao · Fangping Yan · Tianxiang Chen · Shuaishuai Zhang · Shuai Jiang

Received: 23 May 2022 / Accepted: 20 October 2022 / Published online: 31 October 2022
© The Author(s), under exclusive licence to Springer Nature B.V. 2022

Abstract The revolute pair and translational pair are the two most important kinematic pairs in planar mechanism. Their clearances directly affect the accuracy of planar mechanism. In addition, flexible components will also lead to a certain degree of vibration and shaking of the mechanism, which will seriously affect the stability. In this paper, considering the coupling effect of revolute clearance pair, translational clearance pair and elastic deformation of components, an accurate dynamic modeling method of rigid-flexible coupling multi-link mechanism (MLM) considering revolute clearance and translational clearance is proposed to accurately predict the nonlinear behavior. Clearance models of revolute pair and translational pair are established, the flexible element model is established based on the absolute node coordinate formulation (ANCF), and the nonlinear dynamic equation of rigid-flexible coupling six-bar

mechanism considering the clearance of revolute pair and translational pair is built by Lagrange multiplier method (LMD). Dynamic response and chaos identification are researched. Chaos identification is determined qualitatively and quantitatively by phase diagram, Poincaré map and largest Lyapunov exponent. Influences of different clearance values and driving speeds on nonlinear dynamic behavior of mechanism are discussed. Bifurcation diagrams varying with clearance size and driving velocity are studied, respectively. Dynamic modeling method is compared and verified by ADAMS. The experimental platform of six-bar mechanism is built to further verify the correctness of theoretical model.

Keywords Revolute clearance · Translational clearance · Rigid-flexible coupling mechanism · Chaos identification · Nonlinear dynamic

L. Xiao · S. Zhang · S. Jiang (✉)
Department of Electrical and Information, Shandong University of Science and Technology, Jinan 250031, Shandong Province, China
e-mail: jiang_jackson@163.com

F. Yan
College of Mechanical and Electronic Engineering, Shandong University of Science and Technology, Qingdao 266590, China

T. Chen
Qingdao Iron Man Technology Co., Ltd, Qingdao 266590, China

1 Introduction

Revolute pair and translational pair are the important connecting parts of the planar mechanism. Due to manufacturing tolerance and wear, revolute pair and translational pair are not perfect, and there will be some clearances [1–7]. Clearances will affect dynamic response and result in significant deviation between the expected behavior and the actual results. When the mechanism moves too fast or the cross-sectional area

is too small, a certain elastic deformation of the components will be produced. The impact phenomenon related to clearance and the vibration phenomenon related to elastic deformation of components directly affect the service life of mechanism. In addition, joint clearance and elastic deformation of components are the key factors leading to chaos in multi-body system. The chaotic quantization of mechanical system not only helps to understand the nonlinear nature of the system, but also helps to rationalize the control parameters. Besides, the treatment of kinematic pair clearance and elastic deformation of components is a complex and important problem [8–14]. Therefore, it is necessary to research in detail the coupling action between flexible member and clearance, and the influence of this coupling effect on nonlinear dynamics.

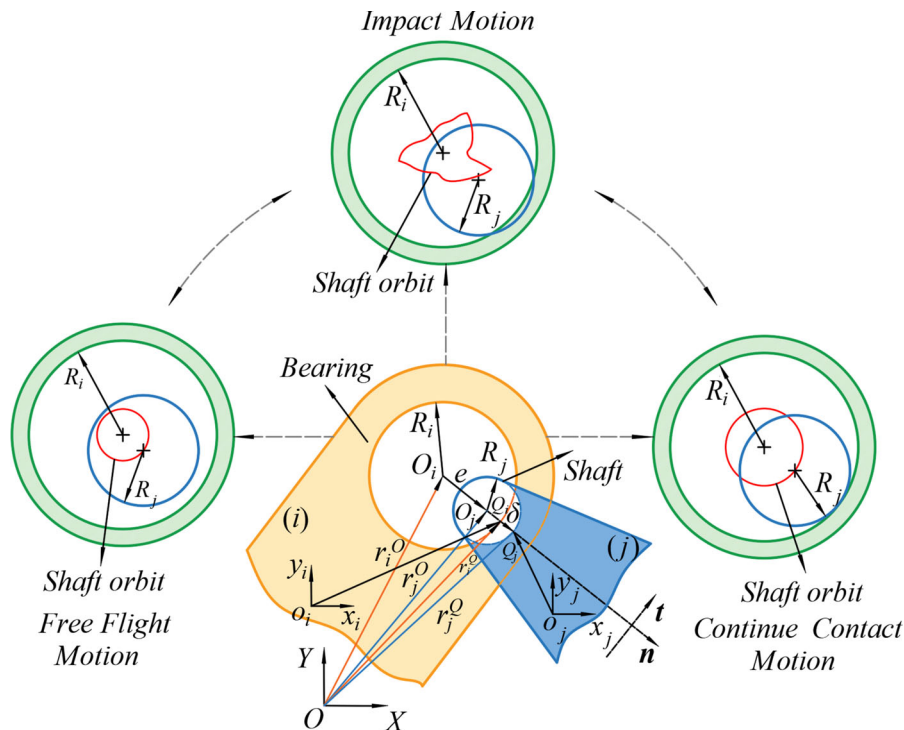
Revolute pair is the most common kinematic pair in planar mechanism. Its clearance will influence the mechanism's stability, which has attracted the attention of many scholars [15–22]. Chen et al. [23] derived a dynamic model of six bars rigid mechanism containing revolute clearance. Marques et al. [24] considered the comprehensive influences related to radial and axial displacement, and proposed a method of dynamic modeling of 3D rotating clearance. Wan et al. [25] built computational dynamic equation of momentum wheel assembly by considering the influencing factors such as flexibility and clearance. Based on fractal theory, Li et al. [26] established a new stiffness coefficient model considering the surface roughness, which considered the elastic, elastic-plastic and plastic deformations of the asperities of the contact surface. Bai et al. [27] introduced a 3D rotating clearance joint modeling method, and its application in satellite antenna system was studied. Alshaer et al. [28] discussed influence of lubrication clearance on motion characteristic and force condition of mechanism. Xu et al. [29] studied the wear characteristic of rotating clearance pair through numerical simulation and experiment.

Any component is an elastomer with different rigidity, and the flexibility of member seriously affects the mechanism's stability. Therefore, many scholars have studied the coupling effect between the revolute clearance pair and elastic deformation of components [30–37]. Pi et al. [38] proposed a unified geometric model of clearance pair within the framework of iso-geometric analysis (IGA). Numerical simulation was

carried out for different flexible mechanism, and their dynamic responses were analyzed in detail. Jiang et al. [39] used the transverse and torsional spring system to describe the dynamics of connected beams containing two clearances, and proposed an improved numerical method to solve dynamic equations by Newmark integral method. Chen et al. [40] researched the effect of operating parameters on dynamics of high-precision mechanism with clearance through mathematical statistical parameters. Xiang et al. [41] studied dynamic of robot manipulator considering parameter uncertainty and clearance. Based on Chebyshev polynomial method, interval algorithm was utilized to calculate the dynamic response of mechanism. Li et al. [42] comprehensively studied effect of clearance and friction coefficient on dynamic of plane deployable structure composed of shear like elements. Chen et al. [43] put forward a novel contact force entropy weight method to evaluate the influences of different clearances and angular velocities on contact force. Chen et al. [44] proposed a dynamic modeling method considering plane rotating clearance pair, elastic deformation and large-scale motion. Li et al. [45] researched dynamic and wear characteristics of solar cell array system containing the revolute clearance and solid coating.

The translational pair is an important connecting part of end effector of planar mechanism, and its clearance seriously affects the motion characteristic of the mechanism, which has been studied by some scholars. Stoenescu et al. [46] discussed the dynamic of planar rigid linkage containing sliding joint clearance and studied the effect of driving velocity and recovery coefficient on chaotic characteristics. Wu et al. [47] proposed an improved model to evaluate the contact force generated by translational clearance, and numerically studied a rigid-body double crank mechanism considering translational clearance. Flores et al. [48] used multiple friction unilateral constraints to model the clearance of translational pair, and proposed and discussed a dynamic modeling approach for crank slider with translational clearance joint. Qian et al. [49] built a 3D translational pair model with clearance, studied the motion between the guide rail and slider. Flores et al. [50] established dynamic equation containing single translational clearance, and the effects of four clearance sizes on mechanism were compared.

Fig. 1 Clearance model of revolute pair



The combined action of revolute clearance and translational clearance can more accurately predict mechanism's dynamics. Chen et al. [51] established the rigid dynamic equation containing multiple clearances by LMD. Wang et al. [52] built rigid dynamic equation of crank slider mechanism with both rotating clearance pair and translational clearance pair. Wu et al. [53] introduced the compound action of translational clearance and rotational clearance on the dynamic of plane rigid crank slider mechanism with correlation dimension and bifurcation.

To sum up, the researches on dynamic behavior of mechanisms with clearance mainly focused on dynamic behavior of rigid / rigid flexible coupling mechanisms with revolute clearance pair, rigid mechanisms with translational clearance pair and rigid mechanisms with mixed clearances. There are few studies on the influence of the hybrid clearance composed of revolute clearance and translational clearance on dynamic response and chaos of rigid flexible coupling MLM. Therefore, the main innovation of this paper is to propose an accurate dynamic modeling method of MLM considering the coupling effects of revolute clearance, translational clearance

and flexibility of the component, and study its dynamic response and chaotic characteristics.

The main arrangements are as follows: in the second section, the models of revolute clearance, translational clearance and flexible member are built, and the accurate nonlinear dynamic model of MLM considering the coupling action of revolute clearance, translational clearance and elastic deformation of member is established. In the third section, dynamic response and chaotic characteristics of rigid-flexible coupling MLM with revolute clearance and translational clearance are analyzed. The experimental platform of six-bar mechanism is built to verify the correctness of theoretical model. Sect 3 gives some conclusions.

2 Dynamic model of rigid-flexible coupling MLM with revolute clearance and translational clearance

2.1 Clearance model of revolute pair

Clearance model of revolute joint and motion state of clearance shaft in bearing are shown in Fig. 1. O_i and

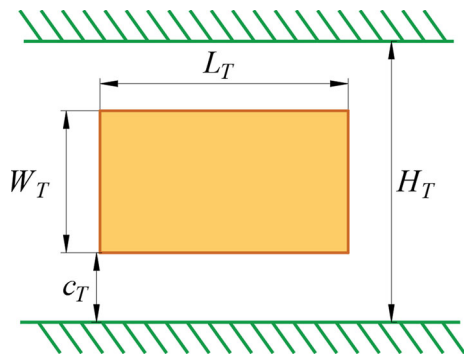


Fig. 2 The clearance model of translational pair

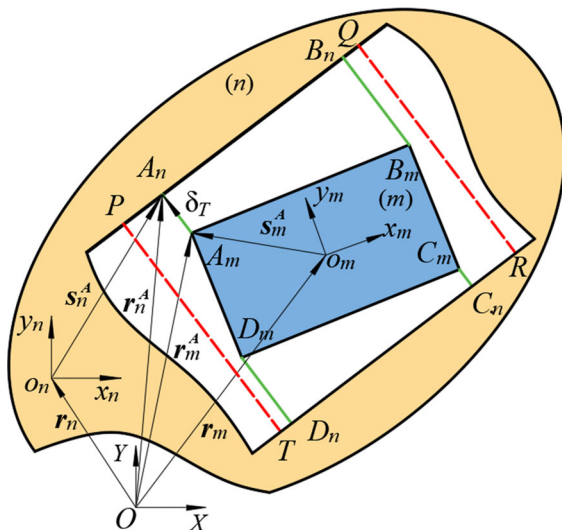


Fig. 3 Analytical model of translational clearance

O_j are the center of bearing and shaft, respectively. R_i is the bearing radius and R_j is the shaft radius. Q_i is the impact point of the bearing during the collision, and Q_j is the impact point on the shaft during the collision.

The eccentric position vector between bearing and shaft is

$$e = r_j^O - r_i^O \tag{1}$$

The relative embedded depth between bearing and shaft is

$$\delta_R = e - c_R \tag{2}$$

where e is magnitude of eccentric position vector, $e = \sqrt{e^T e}$; c is clearance value between bearing and shaft, $c_R = R_i - R_j$.

Motion state of the clearance pair can be determined according to the relative penetration depth

$$\begin{cases} \delta_R > 0, & \text{impact state} \\ \delta_R = 0, & \text{continue contact state} \\ \delta_R < 0, & \text{free flight state} \end{cases} \tag{3}$$

Collision detection at the clearance can be carried out by monitoring the embedded depth. When two components of pair are in contact, the embedded depth has a positive value, while in free flight mode, the symbol is opposite. The change of contact status between shaft and bearing is [42]

$$\delta_R(t_n)\delta_R(t_{n+1}) < 0 \tag{4}$$

When $\delta_R(t_n)\delta_R(t_{n+1}) < 0$, $\delta_R(t_n) < 0$ and $\delta_R(t_{n+1}) > 0$, at this moment, motion state changes from free flight state to impact state. When $\delta_R(t_n)\delta_R(t_{n+1}) < 0$, $\delta_R(t_n) > 0$ and $\delta_R(t_{n+1}) < 0$, at this moment, motion state changes from impact state to free flight state.

Because the Lankarani–Nikravesh model considers the elastic properties and energy dissipation of the colliding object, it is widely used to describe the local collision contact phenomenon, it can be expressed as [11]

$$F_n = K\delta_R^n + D\dot{\delta}_R \tag{5}$$

F_n is normal contact force, K is stiffness coefficient, D is damping coefficient of contact collision, and $\dot{\delta}_R$ is relative velocity of contact collision.

Stiffness coefficient of the contact object is [27]

$$K = \frac{4E_i E_j}{3(E_i(1 - \nu_i^2) + E_j(1 - \nu_j^2))} \left(\frac{R_i R_j}{R_i - R_j} \right)^{\frac{1}{2}} \tag{6}$$

where ν_k ($k = i, j$) and E_k ($k = i, j$) are Poisson’s ratio and Young’s modulus of bearing and shaft, respectively.

Damping coefficient is expressed as

$$D = \frac{3K(1 - c_e^2)\delta_R^{1.5}}{4\dot{\delta}_R^{(-)}} \tag{7}$$

where c_e is coefficient of recovery, $\dot{\delta}_R^{(-)}$ is initial relative velocity.

In addition, the friction between shaft and bearing surface is a complex nonlinear factor of clearance pair.

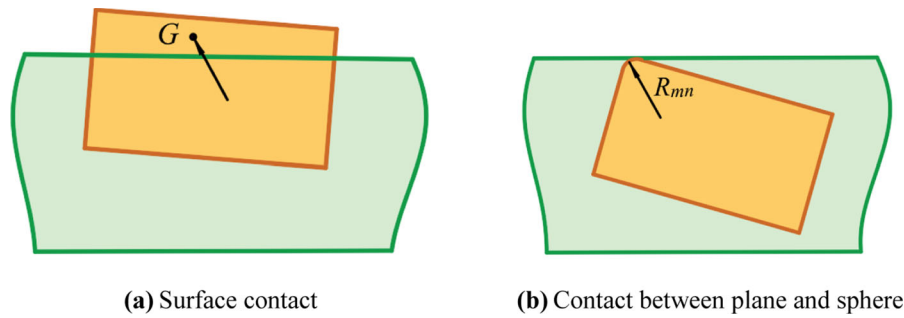


Fig. 4 Contact mode of translational clearance

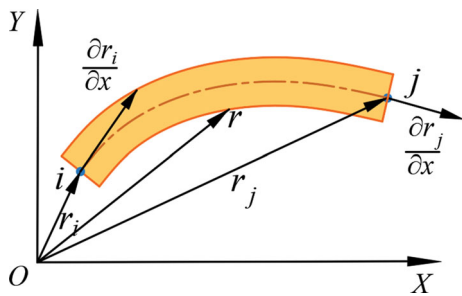


Fig. 5 Flexible beam element model

In order to accurately describe friction, the modified Coulomb friction model is adopted [54]

$$F_t = -\mu_d c_d F_n \frac{v_t}{|v_t|} \tag{8}$$

where μ_d is frictional coefficient; c_d is correction factor; it can be expressed as

$$c_d = \begin{cases} 0, & |v_t| < v_0 \\ \frac{|v_t| - v_0}{v_1 - v_0}, & v_0 \leq |v_t| \leq v_1 \\ 1, & |v_t| > v_1 \end{cases} \tag{9}$$

where v_0 and v_1 are given tolerances for the tangential velocity, $v_0 = 0.0001$ m/s and $v_1 = 0.001$ m/s [44]. When $|v_t| < v_0$, the value of c_d is 0; When $v_0 \leq |v_t| \leq v_1$, the value of c_d is $\frac{|v_t| - v_0}{v_1 - v_0}$; When $|v_t| > v_1$, the value of c_d is 1.

2.2 Clearance model of translational pair

The clearance model of translational pair is shown in Fig. 2. Length and width of slider are L_T and W_T , respectively, the width of guide rail is H_T , the clearance value of the translational pair is

$$c_T = \frac{H_T - W_T}{2} \tag{10}$$

The analysis model of translational clearance is shown in Fig. 3. The slider and the guide rail are represented by m and n . As shown in Fig. 3, A_m, B_m, C_m and D_m are the four corners of the slider, and A_n, B_n, C_n and D_n are the points closest to the corner of slider on the guide rail. The point A is taken as an example for detailed modeling and analysis. The position vector of any point H is

$$r_i^H = r_i + A_i s_i^H (i = m, n) \tag{11}$$

where r_i is position vector of the centroid of component i , A_i is transformation matrix, S_i^H is position vector of any point H .

Position vector between A_m point and the A_n point can be expressed as

$$\delta_T = r_n^A - r_m^A \tag{12}$$

Normal vector of guide rail surface is

$$n_T = (t_T^y \quad -t_T^x)^T \tag{13}$$

where t_T^x and t_T^y are the components of tangential vector t_T in the X and Y directions, respectively.

When there is a collision between two component, the condition of collision between slider and guide rail is [11]

$$n_T^T \delta_T < 0 \tag{14}$$

As shown in Fig. 4a, when the two adjacent corners of slider are in contact with guide rail, collision force acts on the centroid of embedded area, it can be expressed as [50, 52]

$$F_T^n = K_T \delta_T \tag{15}$$

$$K_T = \frac{aE_m E_n}{0.475(E_n(1 - v_m^2) + E_m(1 - v_n^2))} \tag{16}$$

where $\delta_T = \sqrt{\delta_T^T \delta_T}$, a is half of the circumference of rectangular contact surface, E_k ($k = m, n$) and v_k ($k = m, n$) are elastic modulus and Poisson's ratio of slider and guide rail, respectively.

As shown in Fig. 4b, when one or two opposite corners of slider are in contact with guide rail surface, contact force can be expressed as [51]

$$F_T^n = K_T \delta_T^n + D_T \dot{\delta}_T \tag{17}$$

$$K_T = \frac{4E_m E_n \sqrt{R_{mn}}}{3(E_n(1 - v_m^2) + E_m(1 - v_n^2))} \tag{18}$$

where R_{mn} is radius of curvature of slider corner, D_T is damping coefficient, $D_T = \frac{3K_T(1 - c_e^2)\delta_T^{1.5}}{4\delta^{(-)}}$.

The modified Coulomb friction model is also applied to describe the friction of translational clearance, as shown in Eq. (8).

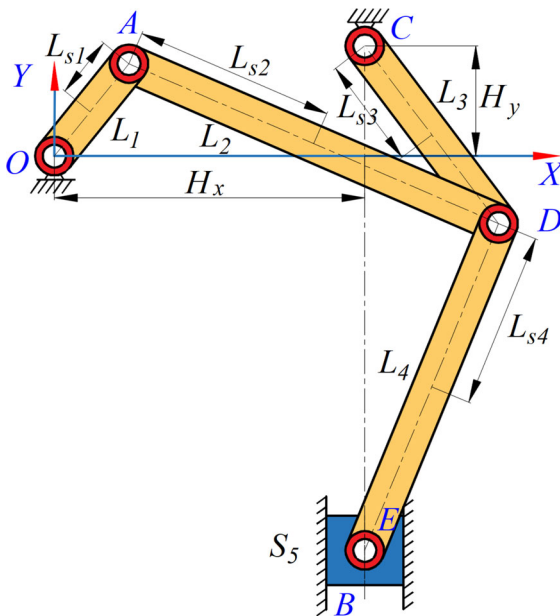


Fig. 6 The schematic diagram of six-bar mechanism

2.3 Flexible beam element model

Flexible beam element model is built by ANCF, as shown in Fig. 5. The position vector of any point on element is

$$r = (r_x \quad r_y)^T = \begin{pmatrix} a_0 + a_1x + a_2x^2 + a_3x^3 \\ b_0 + b_1x + b_2x^2 + b_3x^3 \end{pmatrix} = S_f q_f \tag{19}$$

where S_f is shape function.

$$S_f = (S_f^1 I, S_f^2 I, S_f^3 I, S_f^4 I) \tag{20}$$

where I is the element matrix; $S_f^1 = 1 - 3\zeta^2 + 2\zeta^3$, $S_f^2 = l(\zeta - 2\zeta^2 + \zeta^3)$, $S_f^3 = 3\zeta^2 - 2\zeta^3$, $S_f^4 = l(-\zeta^2 + \zeta^3)$, $\zeta = x/l$, l is length of flexible beam element, q_f is the generalized coordinates of the flexible beam element.

q_f can be expressed as [31]

$$q_f = (q_{f1}, q_{f2}, q_{f3}, q_{f4}, q_{f5}, q_{f6}, q_{f7}, q_{f8})^T = \left(r_{ix}, r_{iy}, \frac{\partial r_{ix}}{\partial x}, \frac{\partial r_{iy}}{\partial x}, r_{jx}, r_{jy}, \frac{\partial r_{jx}}{\partial x}, \frac{\partial r_{jy}}{\partial x} \right)^T \tag{21}$$

where (r_{ix}, r_{iy}) and (r_{jx}, r_{jy}) are the position vectors of nodes i and j , respectively; $\left(\frac{\partial r_{ix}}{\partial x}, \frac{\partial r_{iy}}{\partial x} \right)$ and $\left(\frac{\partial r_{jx}}{\partial x}, \frac{\partial r_{jy}}{\partial x} \right)$

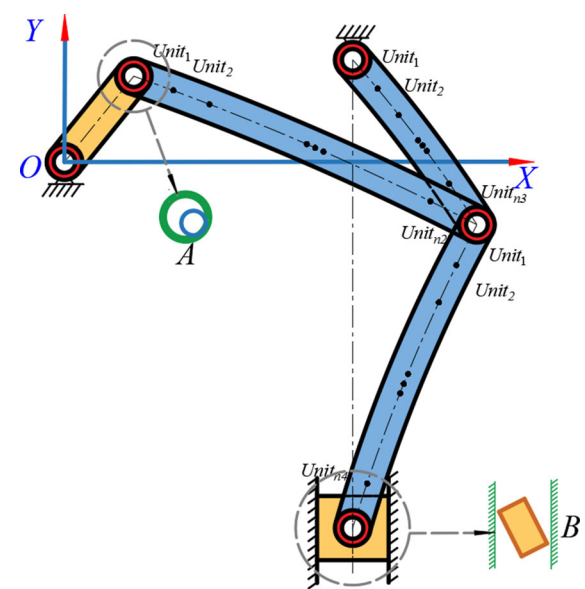


Fig. 7 The schematic diagram of mechanism with revolute clearance and translational clearance

represent slope vectors in the tangential direction of the axis.

Kinetic energy of flexible beam element is

$$T_f = \frac{1}{2} \int_V \rho \dot{\mathbf{r}}^T \dot{\mathbf{r}} dV = \frac{1}{2} \dot{\mathbf{q}}_f^T \left(\int_V \rho S_f^T S_f dV \right) \dot{\mathbf{q}}_f = \frac{1}{2} \dot{\mathbf{q}}_f^T \mathbf{M}_f \dot{\mathbf{q}}_f \tag{22}$$

where M_f is mass matrix, $M_f = \int_V \rho S_f^T S_f dV$. ρ and V are the density and volume.

The element elastic force of flexible beam is [45]

$$\mathbf{F}_f = \frac{\partial U_f}{\partial \mathbf{q}_f} = \frac{\partial (\mathbf{U}_t + \mathbf{U}_l)}{\partial \mathbf{q}_f} = \mathbf{F}_f^t + \mathbf{F}_f^l = \mathbf{K}_f^t \mathbf{q}_f + \mathbf{K}_f^l \mathbf{q}_f \tag{23}$$

where U_f , F_f^t , F_f^l , K_f^t and K_f^l represent the total strain energy, bending elastic force, axial elastic force, bending stiffness and axial stiffness of flexible beam element, respectively.

According to the theory of continuum mechanics, the total strain energy of the element includes bending strain energy and axial tensile strain energy, which can be expressed as [34]

$$U_f = U_l + U_t = \frac{1}{2} \int_0^l E_f A_f \varepsilon_f^2 dx + \frac{1}{2} \int_0^l E_f I_f \kappa_f^2 dx \tag{24}$$

where E_f , A_f , ε_f , I_f and κ_f are the Young’s modulus, cross-sectional area, strain and area moment of inertia and curvature, respectively.

The bending stiffness and the axial stiffness of the flexible beam element are

$$\mathbf{K}_f^t = \int_0^l E_f I_f S_f'^T S_f'' dx \tag{25}$$

$$\mathbf{K}_f^l = \int_0^l E_f A_f \varepsilon_f \bar{S}_f dx \tag{26}$$

where $\bar{S}_f = S_f'^T S_f'$.

Table 1 Geometric and inertial parameters

Component	Length of rod(m)	Mass (kg)	Moment of inertia ($10^{-3} \text{ kg}\cdot\text{m}^2$)
Crank 1	0.075(L_1)	0.751(m_1)	1.408
Rod 2	0.700(L_2)	6.601(m_2)	269.541
Rod 3	0.584(L_3)	5.515(m_3)	156.744
Rod 4	0.450(L_4)	4.261(m_4)	71.904
Slider 5	–	5.776(m_5)	4.813

The flexible beam element equation can be expressed as [54]

$$\mathbf{M}_f \ddot{\mathbf{q}}_f + \mathbf{F}_f = \mathbf{Q}_f \tag{27}$$

where Q_f is the generalized external force.

2.4 Establishment of nonlinear dynamic model of rigid-flexible coupling MLM considering revolute clearance and translational clearance

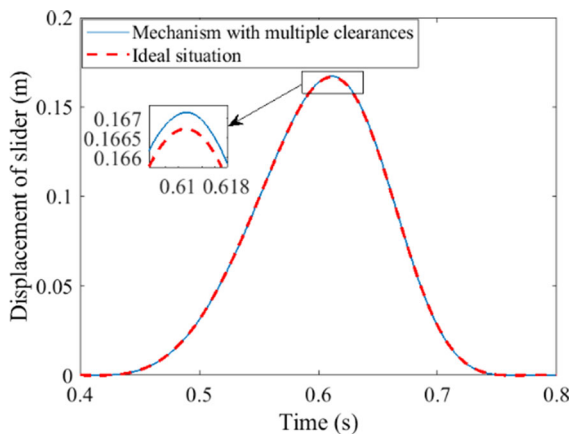
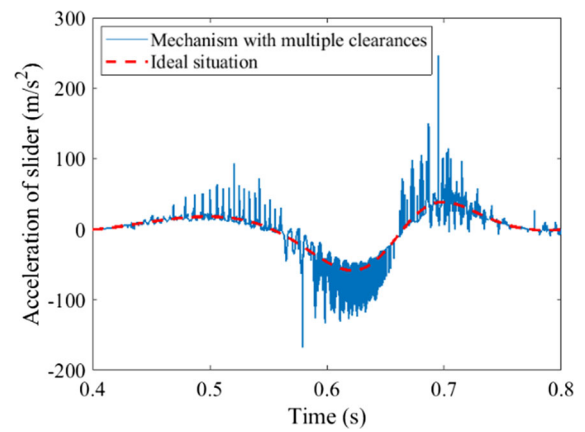
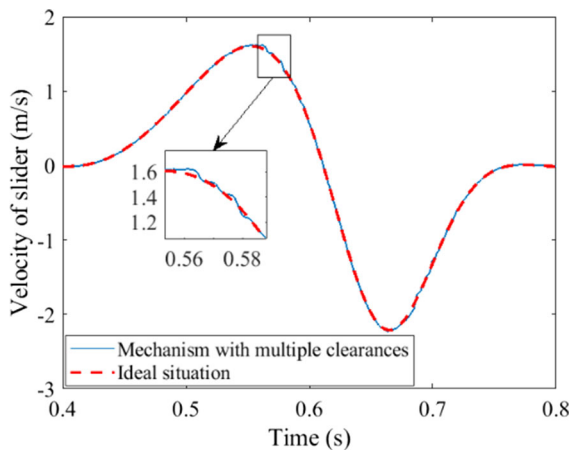
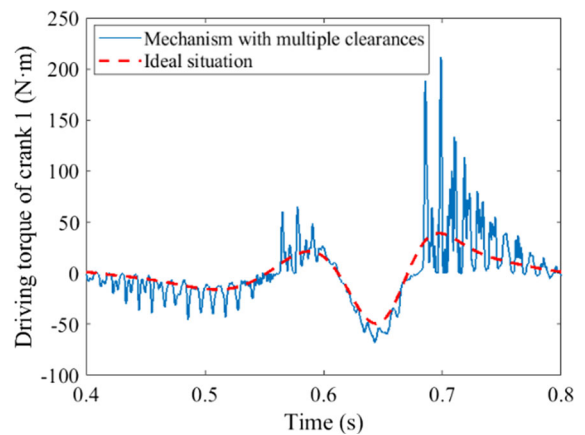
2.4.1 Description of structural features

The schematic diagram of six-bar mechanism is shown in Fig. 6. The mechanism is composed of frame, crank 1 (L_1), connecting rod 2 (L_2), connecting rod 3 (L_3), connecting rod 4 (L_4) and slider 5 (S_5). L_1 and L_2 are connected by revolute joint A. L_4 and S_5 are connected by translational pair B. L_3 and frame are connected by revolute joint C. L_2 , L_3 and L_4 are connected by compound hinge D. L_4 and slider are connected by revolute joint E. The compound hinge D can be regarded as a combination of two revolute pairs (D_1 and D_2). L_2 and L_4 are connected by the revolute pair D_1 , and L_3 and L_4 are connected by revolute pair D_2 . Six-bar mechanism can be better applied to the main transmission mechanism of multi-link press.

As the slider is the end effector of the whole mechanism, the cooperation between the slider and the guide rail is an important factor affecting the dynamic and accuracy for whole mechanism. Therefore, translational clearance B needs to be considered. At the same time, revolute pair A is directly related to the driving member for it is an important connecting part between crank 1 and rod 2. Therefore, it is necessary to pay attention to the revolute clearance pair A between crank 1 and connecting rod 2. In addition, L_2 , L_3 and L_4 are regarded as flexible members for they are longer and more prone to elastic deformation. L_1 is considered a rigid member for its short length and high stiffness. Similarly, the slider is regarded as a rigid

Table 2 Clearance simulation parameters and flexible rod parameters

Parameter	Parameter values	Parameter	Parameter values
Bearing radius(R_1)	15(mm)	Friction coefficient(c_f)	0.15
Restitution coefficient(c_e)	0.9	Young modulus(E_f)	207(GPa)
Length of slider(L_T)	150(mm)	Cross section area(A_f)	$0.06 \times 0.02(\text{m}^2)$
Width of slider(W_T)	100(mm)	Second moment of area(I)	$4 \times 10^{-8}(\text{m}^4)$
Thickness of slider(T_T)	50(mm)	Density(ρ)	$7801(\text{kg}/\text{m}^3)$
Poisson ratio($\nu_i, \nu_j, \nu_m, \nu_n$)	0.3	Integral tolerance	0.000001
Friction coefficient (c_f)	0.15	Integral step	$0.0001 \times (2\pi/\omega)(\text{s})$

**Fig. 8** Displacement**Fig. 10** Acceleration**Fig. 9** Velocity**Fig. 11** Driving torque

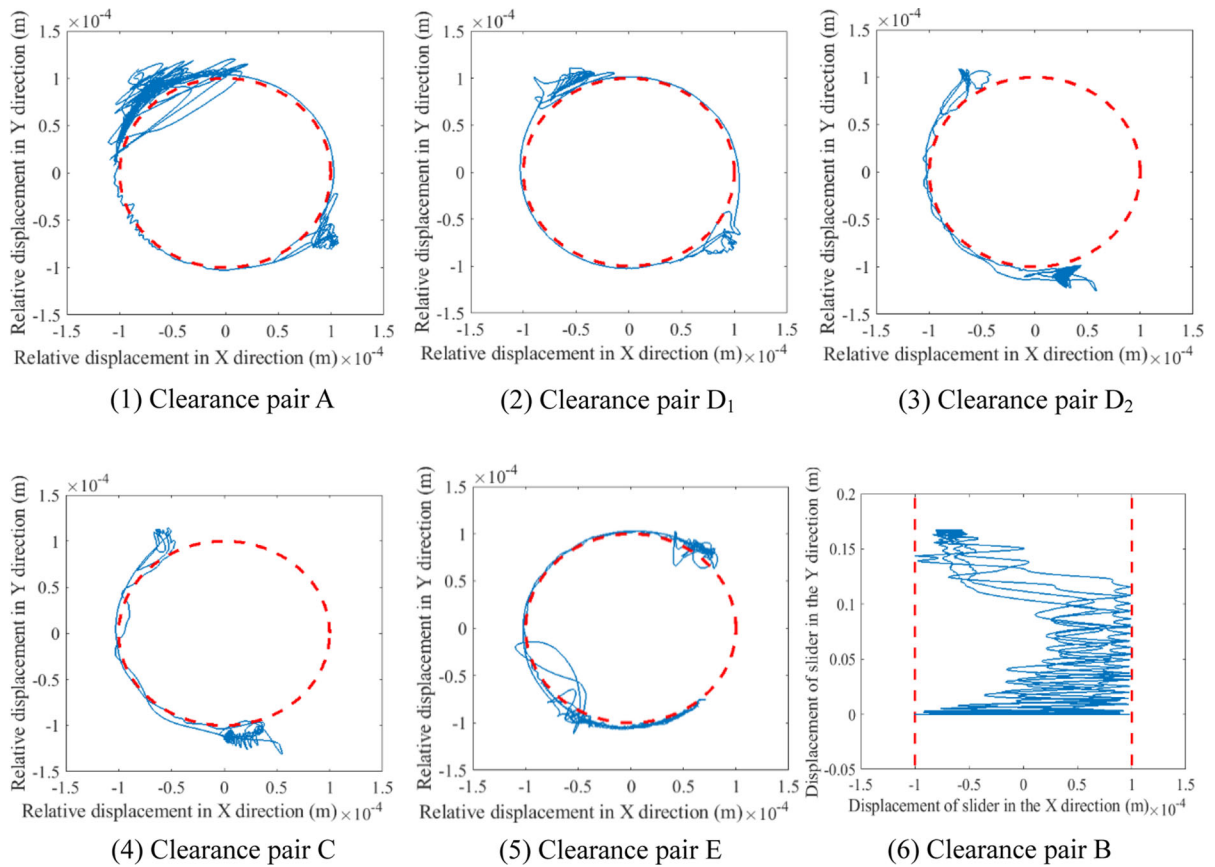


Fig. 12 Trajectory of clearance pair

member for its high stiffness. Therefore, it is very necessary to study dynamic model of MLM considering the coupling action of revolute clearance, translational clearance and flexibility of component. The schematic diagram of rigid-flexible coupling six-bar mechanism with revolute clearance and translational clearance is shown in Fig. 7.

2.4.2 Rigid-flexible coupling dynamic model with revolute clearance and translational clearance

Velocity and acceleration constraint equation can be expressed as [23]

$$\Phi_q \dot{q} = -\Phi_t \equiv v \tag{28}$$

$$\Phi_q \ddot{q} = -(\Phi_{qq} \dot{q}) \dot{q} - 2\Phi_{qt} \dot{q} - \Phi_{tt} \equiv \gamma \tag{29}$$

where Φ_q is Jacobian matrix, $\Phi_q = \partial\Phi/\partial q$, \dot{q} and \ddot{q} are generalized velocity vector and acceleration vector,

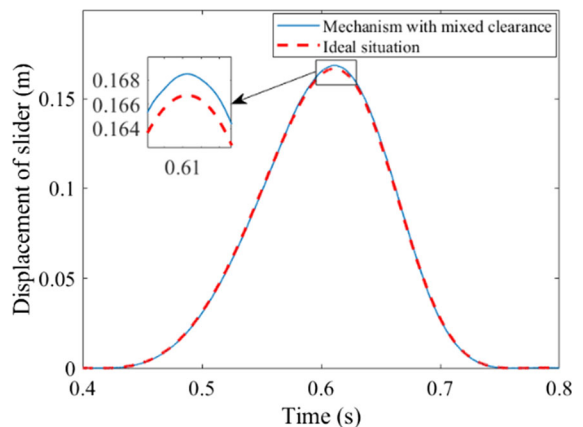


Fig. 13 Displacement

respectively. $\Phi_{qt} = \partial\Phi_q/\partial t$, $\Phi_t = \partial\Phi/\partial t$, $\Phi_{tt} = d\Phi_t/dt$.

Based on LMD, the rigid-flexible coupling dynamic equation containing clearances is [55]

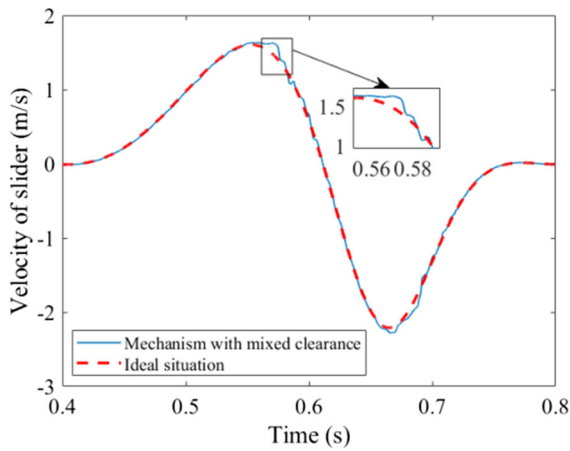


Fig. 14 Velocity

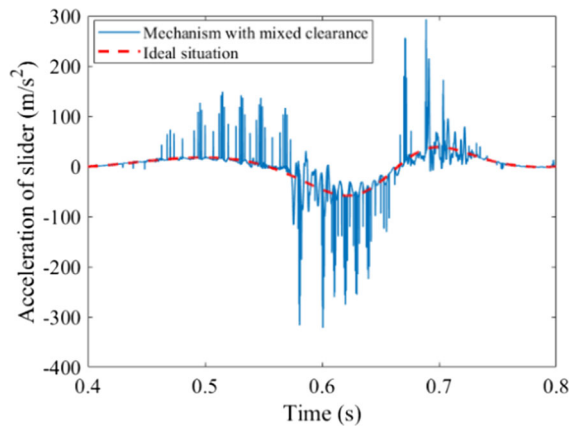


Fig. 15 Acceleration

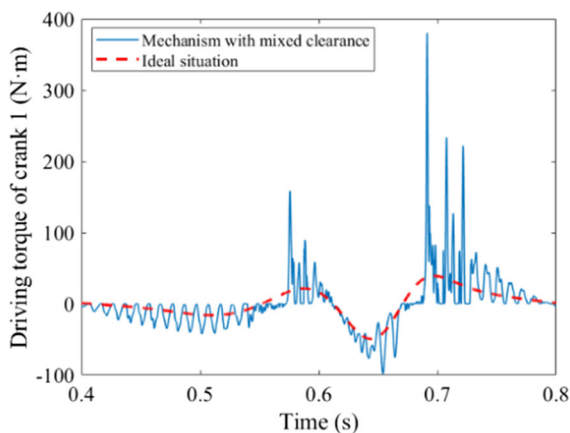


Fig. 16 Driving torque

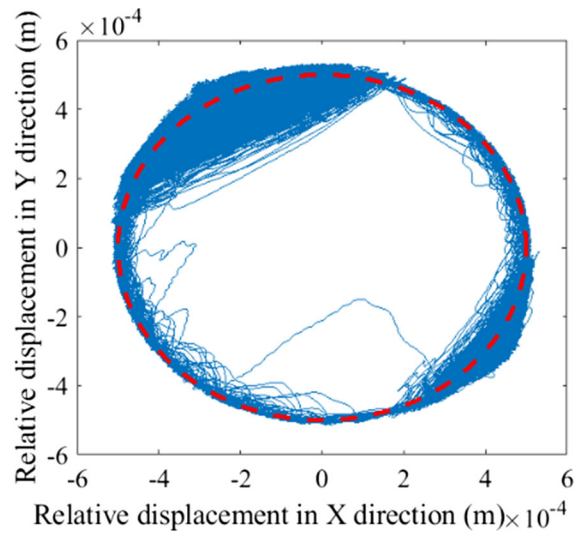


Fig. 17 Trajectory of revolute clearance joint

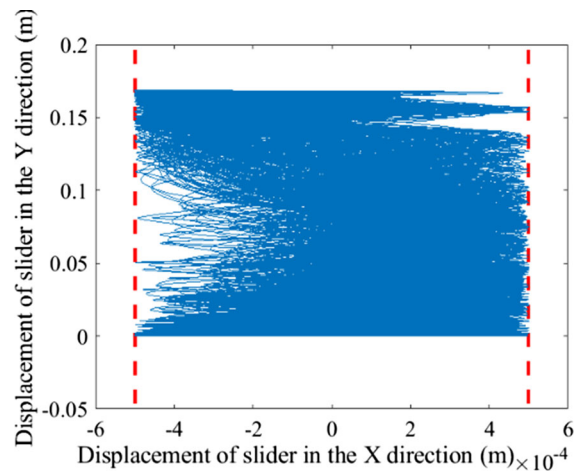


Fig. 18 Trajectory of translational clearance joint

$$\bar{M}_f \ddot{q} + \Phi_q^T \lambda + \bar{F}_f = \bar{Q}_f \tag{30}$$

where \bar{M}_f , λ , \bar{F}_f and \bar{Q}_f are the mass matrix, Lagrange multiplier, elastic force and generalized force of system, respectively.

Baumgarte stabilization technology is used to suppress the acceleration constraint conflict by feedback the position and velocity constraint conflict [24, 47, 56, 57], dynamic equation can be written as

$$\begin{pmatrix} M_f & \Phi_q^T \\ \Phi_q & 0 \end{pmatrix} \begin{pmatrix} \ddot{q} \\ \lambda \end{pmatrix} = \begin{pmatrix} Q_f - F_f \\ \gamma - 2\alpha\dot{\Phi} - \beta^2\Phi \end{pmatrix} \tag{31}$$

3 Nonlinear dynamics behavior analysis of rigid-flexible coupling MLM with revolute clearance and translational clearance

3.1 Structural parameters of system

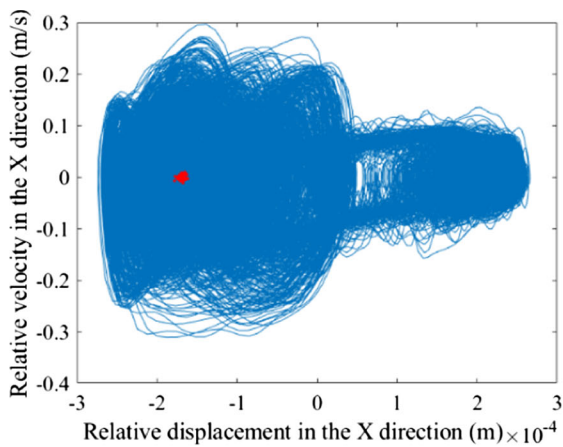
Geometric and inertial parameters are shown in Table 1. Clearance simulation parameters and flexible rod parameters are shown in Table 2.

3.2 Dynamic response analysis of rigid-flexible coupling MLM with multiple clearances

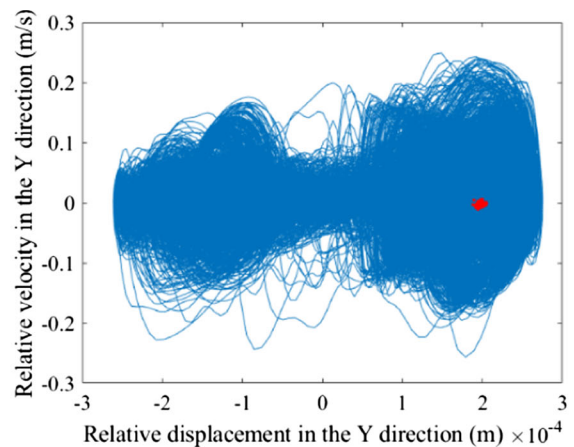
As shown in Fig. 6, the six-bar mechanism has four revolute pairs, one compound hinge and one

translational pair. The revolute pair at point O is used to connect the crank and the motor. The revolute pair at point O is usually subject to interference treatment, and generally no clearance will be generated. Therefore, the clearance is not considered for the revolute pair at O, and the clearances are considered for other kinematic pairs, including revolute clearances A, C and E, compound clearance hinge D, and translational clearance pair B. The clearance values and driving velocity are 0.1 mm and 150 rpm, respectively. Dynamic response diagrams are shown in Figs. 8, 9, 10, 11, 12.

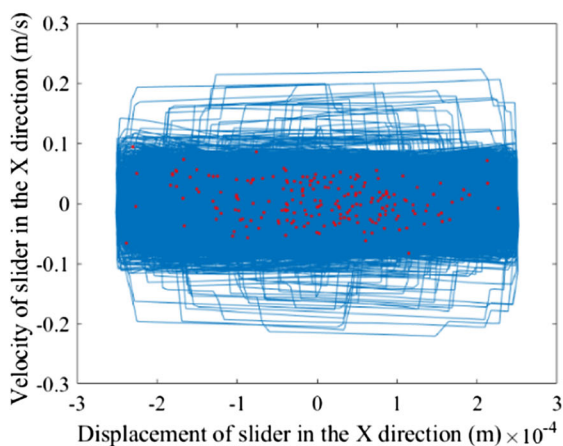
From the displacement, velocity and acceleration curves, the displacement and velocity are less sensitive to the clearance and flexible component, and the



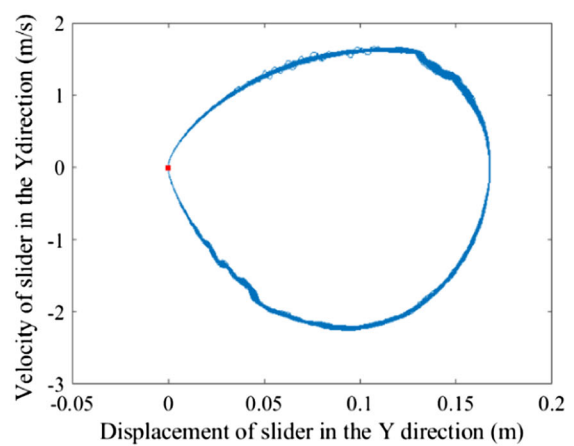
(1) Revolute clearance in X direction



(2) Revolute clearance in Y direction



(3) Translational clearance in X direction



(4) Translational clearance in Y direction

Fig. 19 Phase diagram and Poincaré map

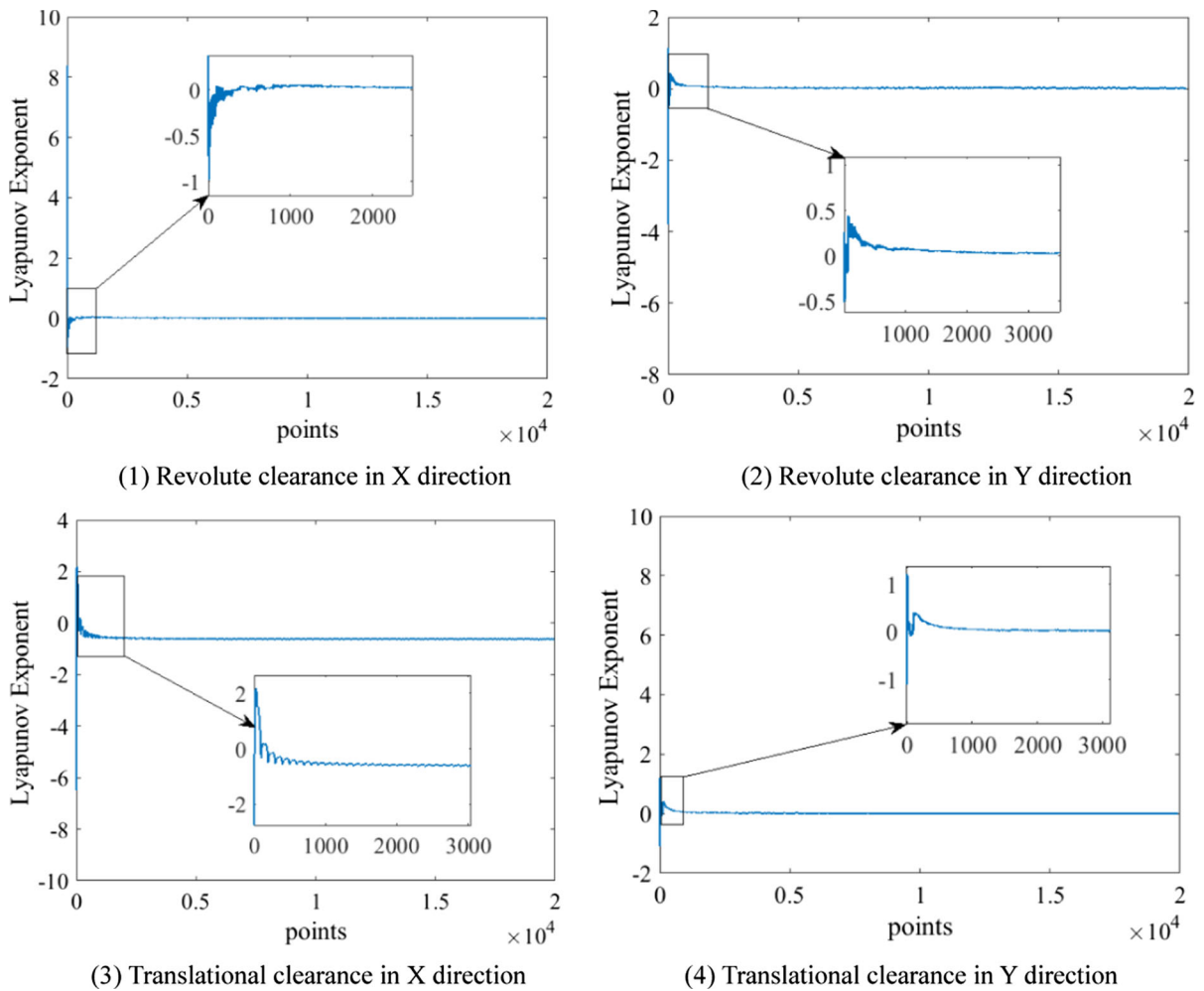


Fig. 20 LLE

Table 3 LLE of clearance joints

	Revolute clearance in X direction	Revolute clearance in Y direction	Translational clearance in X direction	Translational clearance in Y direction
LLE	0.010	0.027	-0.059	0.203

displacement curve almost coincides with the ideal curve, and the velocity curve has a weak vibration near the ideal curve, while the acceleration curve produces a more violent vibration and produces some obvious peaks. The driving torque curve shows that the sensitivity of the torque to the clearance and the flexible rod is also large, and some obvious peaks also appear.

The trajectory diagram shows that the movement of shaft in the bearing and the movement of the slider in the guide rail are disordered. As for the clearance of the revolute pairs, the disorder of the shaft movement in the bearing at the clearance A is greater, and the embedding depth of the shaft in the bearing is greater. When the revolute clearances A, C and E, compound clearance hinge D, translational clearance pair B are

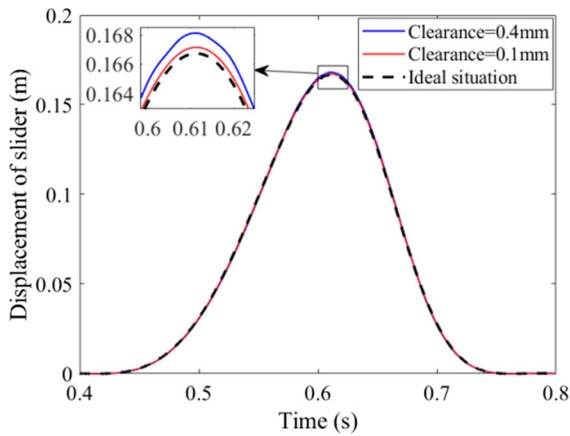


Fig. 21 Displacement

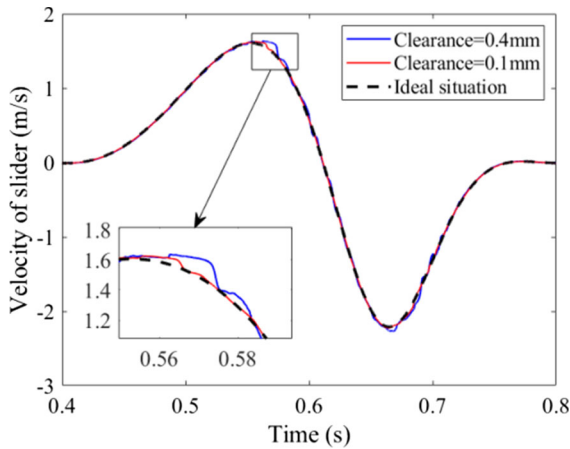


Fig. 22 Velocity

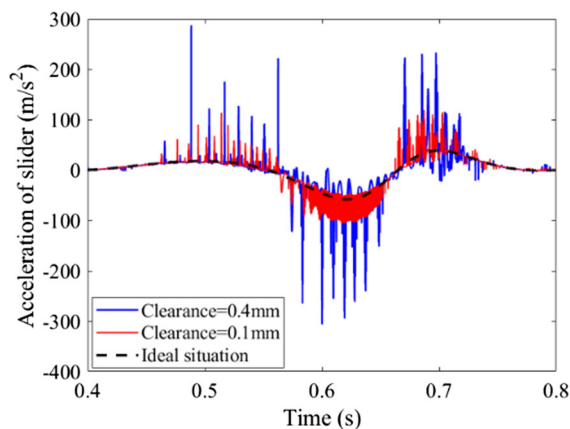


Fig. 23 Acceleration

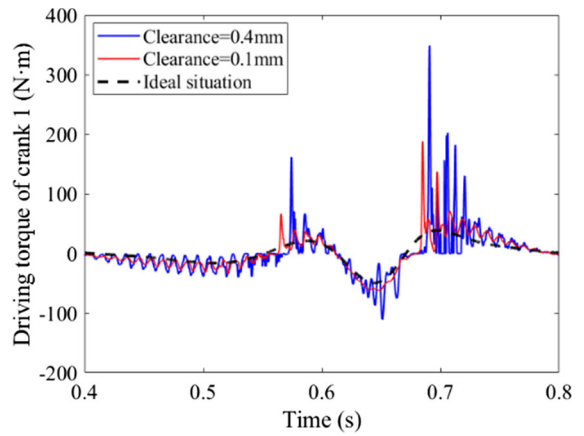


Fig. 24 Driving torque

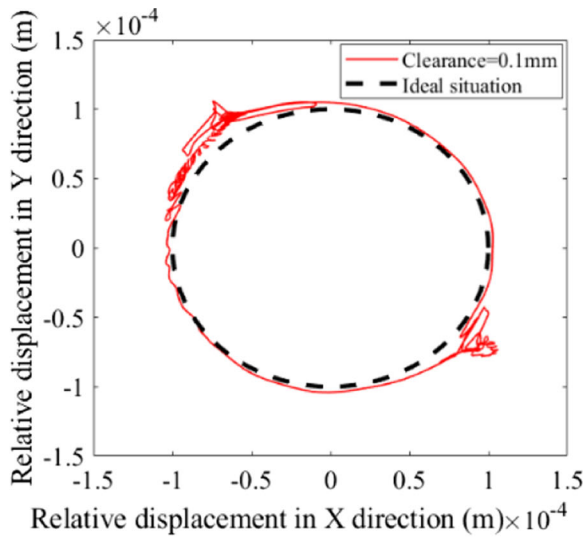
all considered, the nonlinear degree of the dynamic equation is greater and its solving speed is relatively slower. Since the research on the nonlinear characteristics requires a lot of data, in order to facilitate the research on the nonlinear characteristics in the following chapters, the following chapters mainly consider the revolute clearance A and translational clearance B.

3.3 Dynamic response analysis and chaos identification of rigid-flexible coupling MLM with revolute clearance and translational clearance

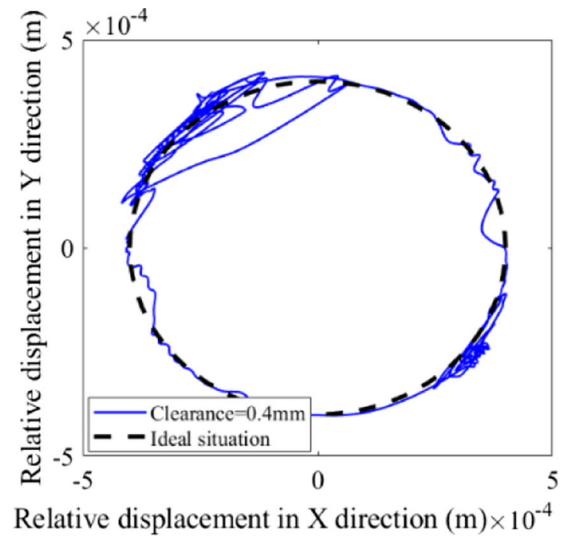
3.3.1 Dynamic response analysis

In order to fully understand the effect of coupling action of revolute clearance pair, translational clearance pair and the flexible component on the mechanism, dynamic response is analyzed in detail, including motion characteristics curve, driving torque curve and center trajectory curve at clearance pair, as shown in Figs. 13, 14, 15, 16, 17, 18, respectively. The clearance value of clearance pair and driving speed of crank are 0.5 mm and 150 rpm, respectively.

From the dynamic response diagram, the coupling action of revolute clearance, translational clearance and elastic deformation of components has a greater impact on acceleration and torque, but less on displacement and velocity. The displacement is almost consistent with the curve under the ideal condition. Through the local enlarged view, there are small fluctuations in velocity, while the acceleration and

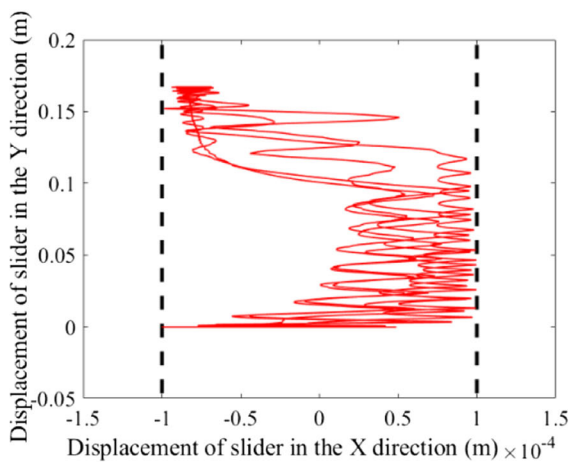


(1) Clearance=0.1mm

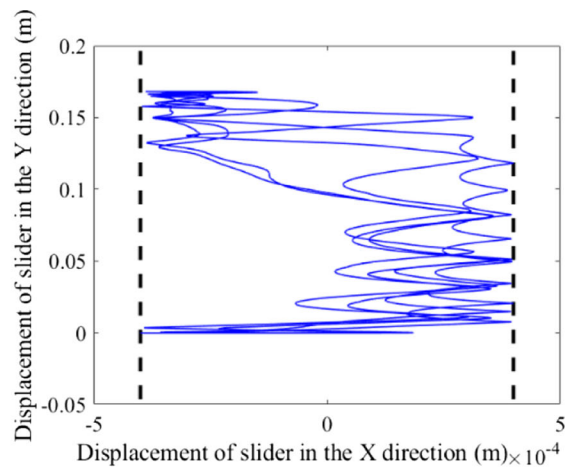


(2) Clearance=0.4mm

Fig. 25 Trajectory of the shaft in the bearing



(1) Clearance=0.1mm



(2) Clearance=0.4mm

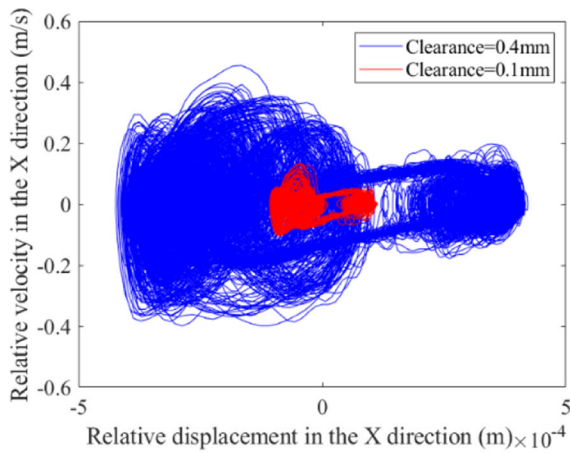
Fig. 26 Trajectory of the slider in the guild rail

Table 4 The maximum peak value of dynamic response under different clearance values

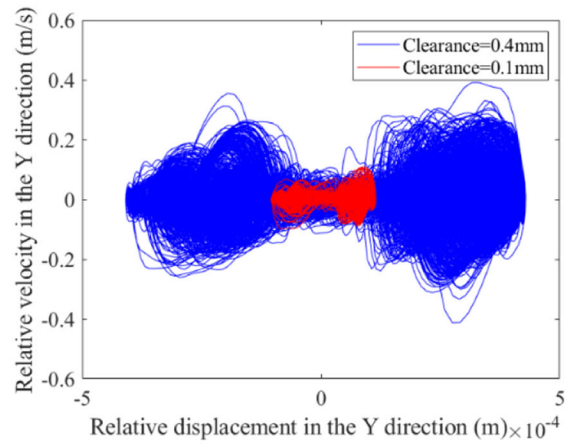
	Clearance value = 0.1 mm	Clearance value = 0.4 mm
Displacement	0.1672 m	0.1681 m
Velocity	-2.209 m/s	-2.266 m/s
Acceleration	119.0 m/s ²	287.3 m/s ²
Torque	188.0 N·m	348.5 N·m

torque have violent vibration and more peaks. The central trajectory curve is the real motion trajectory of the shaft and the slider when the mechanism runs for

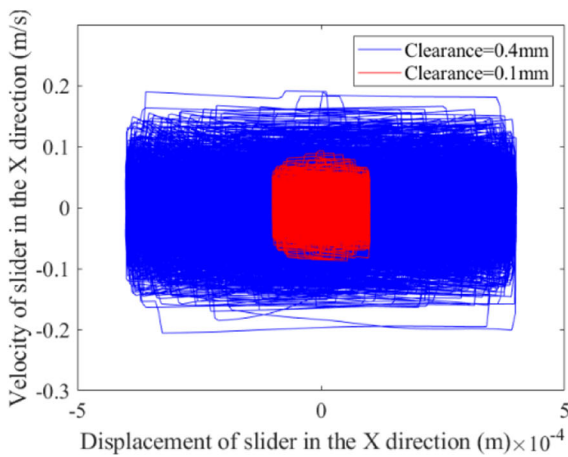
200 cycles. It can be seen that the coupling action of clearance and component flexibility intensifies the collision between the two components at the kinematic



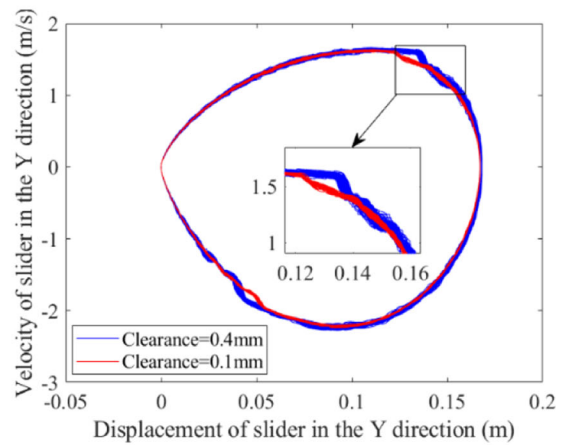
(1) Revolute clearance in X direction



(2) Revolute clearance in Y direction



(3) Translational clearance in X direction



(4) Translational clearance in Y direction

Fig. 27 Phase diagram

pair with clearance, which leads to the instability of the motion state at clearance pair.

3.3.2 Chaos identification

In order to study the effect of revolute clearance, translational clearance and elastic deformation of components on nonlinear characteristics, chaos identification is carried out through phase diagram, Poincaré map and LLE, as shown in Figs. 19, 20, respectively. LLEs of revolute clearance and translational clearance are shown in Table 3.

Through the phase diagram and Poincaré map, it can be qualitatively determined that the revolute

clearance pair is in the chaotic motion state in the X and Y directions, and the translational clearance pair is in the chaotic motion state in the X direction, and the translational clearance pair is in the periodic motion state along the Y direction. Because when LLE is greater than 0, mechanism is in chaotic motion state, and when LLE is less than 0, mechanism is in periodic motion state. LLE can quantitatively determine that the revolute clearance pair is in chaotic motion state in X and Y directions, the translational clearance pair is in chaotic motion state in X direction, and the translational clearance pair is in periodic motion state along Y direction.

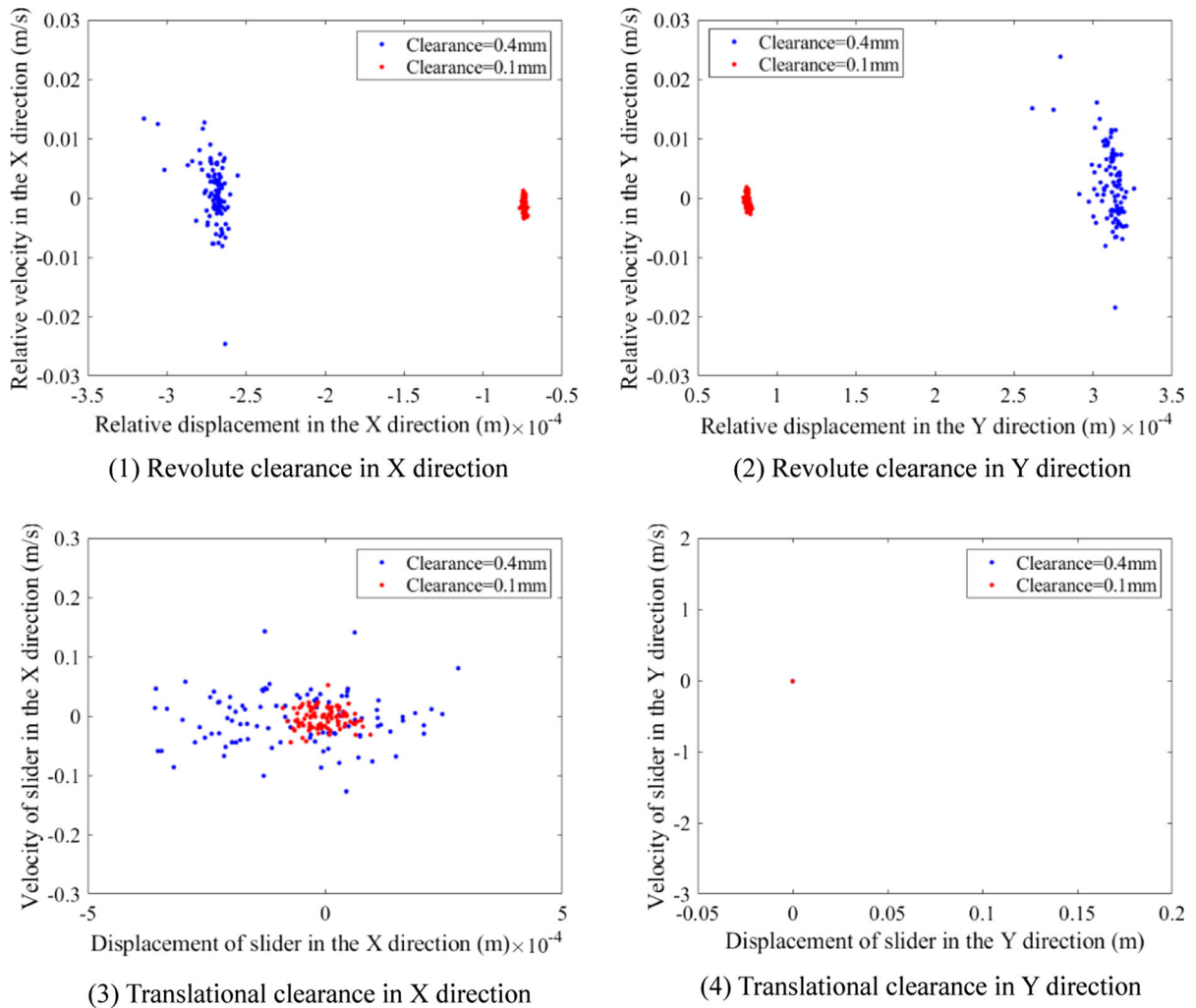


Fig. 28 Poincaré map

3.4 Influence of different clearance values on nonlinear dynamic behavior of rigid-flexible coupling MLM with revolute clearance and translational clearance

3.4.1 Analysis of dynamic response

Two clearance values are selected to study the effect of clearance sizes on dynamic response, which are 0.1 mm and 0.4 mm, respectively. The speed of the driving member is 150 rpm. Dynamic response diagrams are shown in Figs. 21, 22, 23, 24, 25, 26.

According to the displacement and velocity curves, displacement and velocity are less affected by the coupling action of clearance and flexible member, but

the local enlarged diagram shows that the greater the clearance value, the more obvious impact on mechanism. It is obvious from the acceleration curve and torque curve that the larger the clearance value is, the greater the vibration peak value of response is and the more unstable the mechanism is. In addition, acceleration curve shows that the smaller the clearance value, the faster the response vibration frequency, which is mainly caused by the more collision times between the slider and guide rail. The maximum peak value of dynamic response under different clearance sizes is shown in Table 4. The center trajectory diagram shows that the larger the clearance value, the more chaotic the motion state of shaft in the bearing and slider in the guide rail.

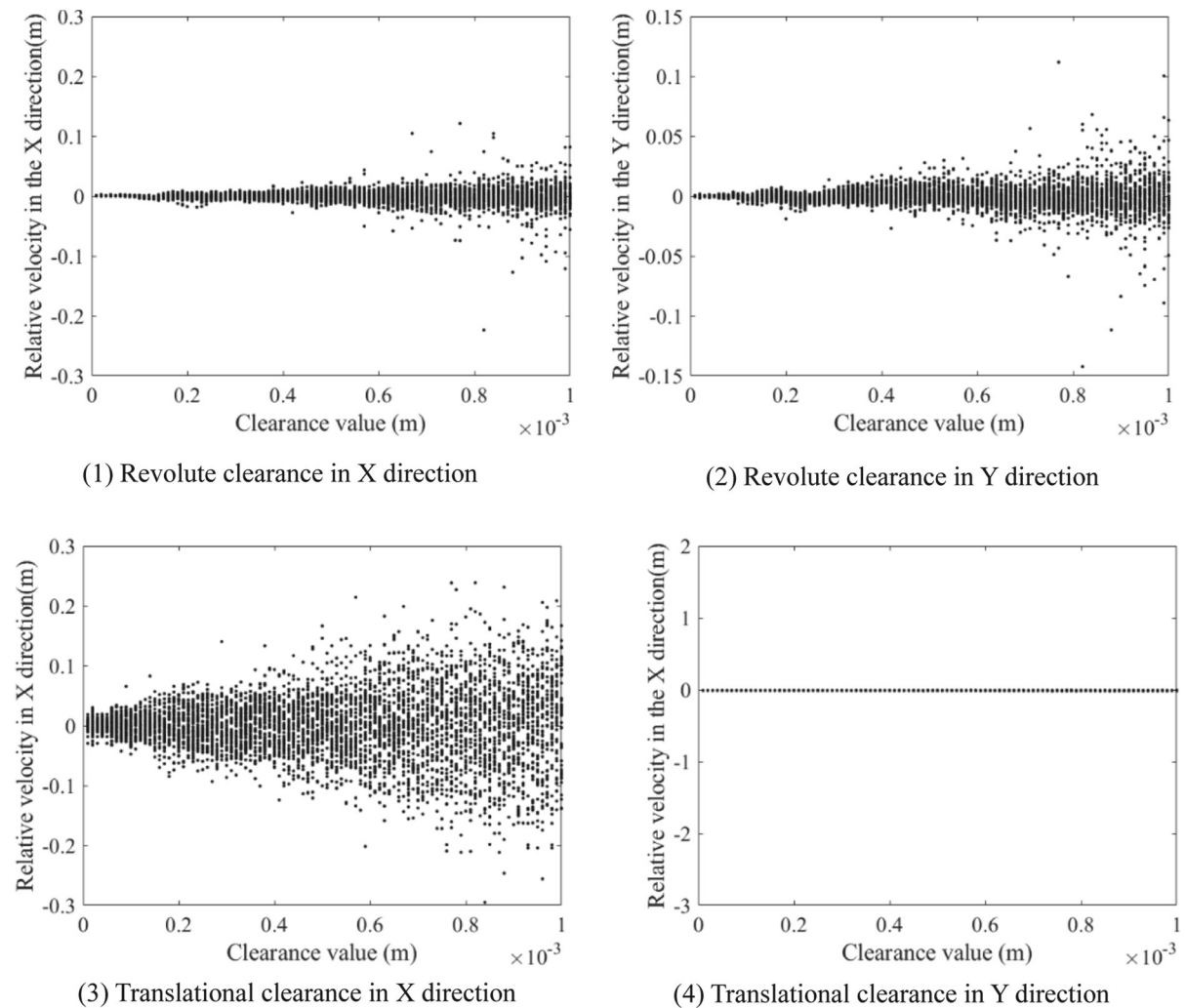


Fig. 29 Bifurcation diagram varying with clearance value

3.4.2 Analysis of nonlinear characteristics

The influence of two clearance values (0.1 mm and 0.4 mm) on the chaotic characteristics is analyzed through the phase diagram and Poincaré map, as shown in Figs. 27, 28, respectively. The bifurcation diagram varying with clearance value is shown in Fig. 29, and the value area of the clearance value is [0 mm, 1 mm].

With the increase of clearance value, the area of phase diagram of revolute clearance pair in the X and Y directions and phase diagram of translational clearance pair in the X direction also increase, their corresponding Poincaré maps also diffuse, and the chaotic phenomenon of the revolute clearance pair in

the X and Y directions and translational clearance pair in the X direction are strengthened. The movement of slider in the Y direction is weakly affected by the clearance value. Through the local enlarged diagram of the phase diagram, the phase diagram also becomes chaotic with the increase of the clearance value, but the Poincaré map is always an isolated point, which shows that the slider moves periodically in the Y direction. According to the bifurcation diagram, with the increase of the clearance value, the chaotic phenomenon of revolute clearance pair in the X and Y directions and the translational clearance pair in the X direction are gradually enhanced, and the chaotic phenomenon of translational clearance pair in the X direction is stronger than that of the revolute clearance

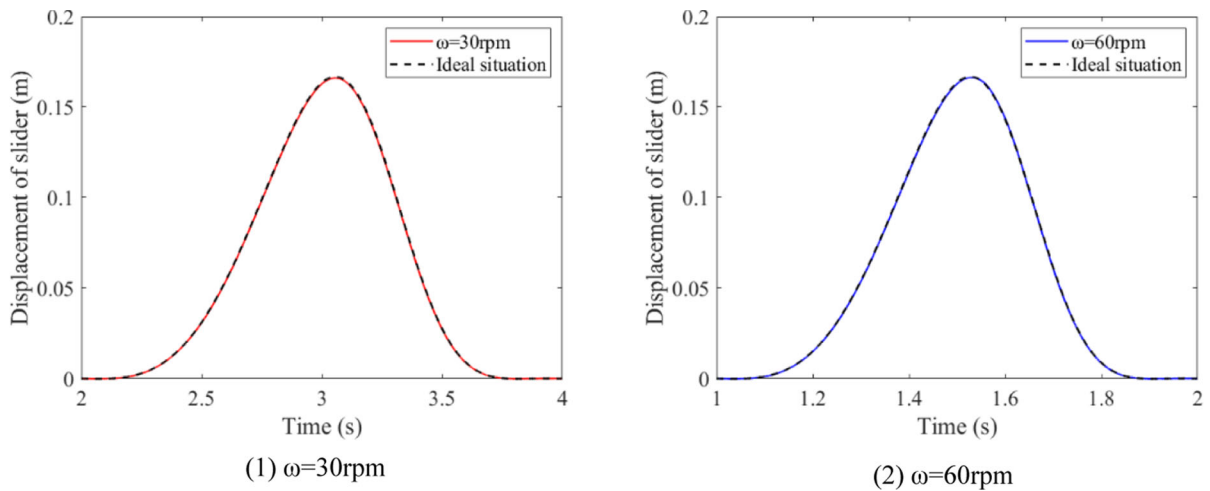


Fig. 30 Displacement of slider

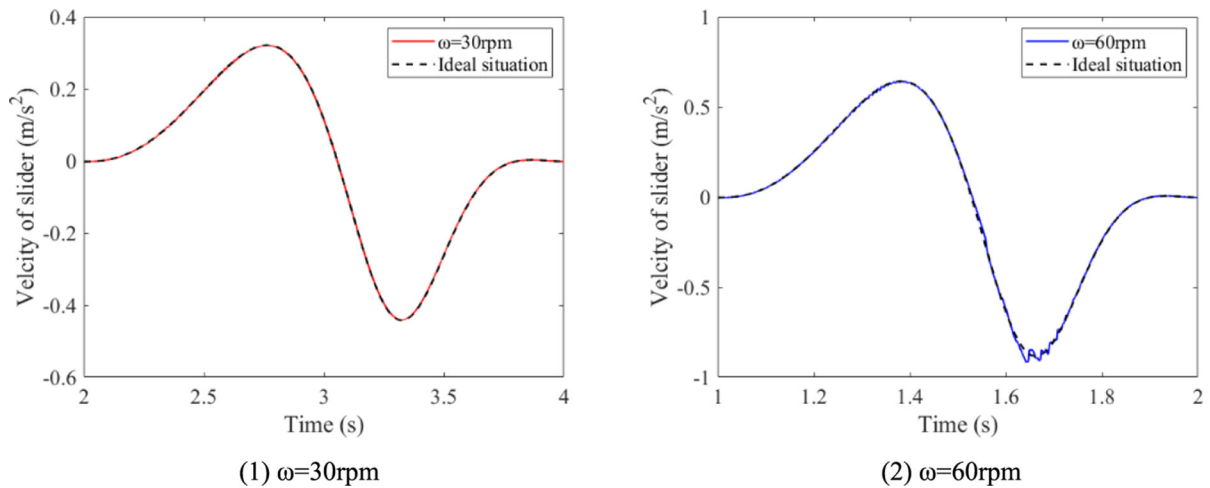


Fig. 31 Velocity of slider

pair in the X and Y directions. The movement of slider in the Y direction is less affected by the clearance value and flexibility of component, so it is always in the state of periodic movement.

3.5 Influence of different speeds on nonlinear dynamic behavior of rigid-flexible coupling MLM with revolute clearance and translational clearance

3.5.1 Analysis of dynamic response

Two different speeds of driving member are selected to research the effect of various speeds on dynamic

response, which are 30 rpm and 60 rpm, respectively. The clearance sizes of revolute pair and translational pair are both 0.2 mm. The dynamic response diagrams are shown in Figs. 30, 31, 32, 33, 34, 35.

Because the sensitivity of displacement to driving speed is not high, there is no obvious fluctuation in displacement curve. The speed curve shows that the speed curve fluctuates significantly around the ideal curve as the driving speed increases. As shown in acceleration curve and driving torque curve, the acceleration and torque are greatly affected by driving speed. The faster the driving speed is, the greater peak value of the response is, and the more unstable the mechanism is. The maximum peak value of dynamic

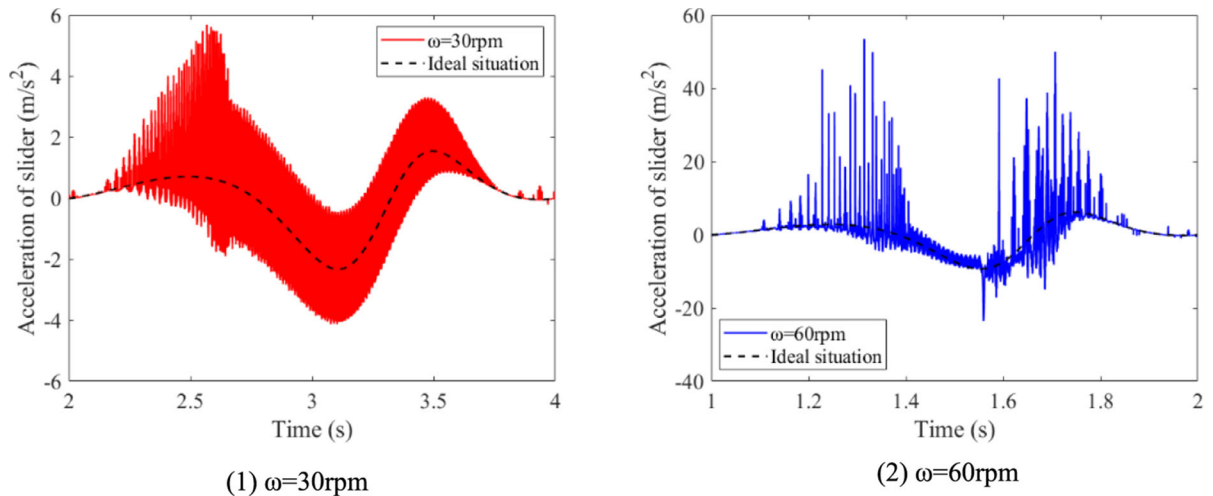


Fig. 32 Acceleration of slider

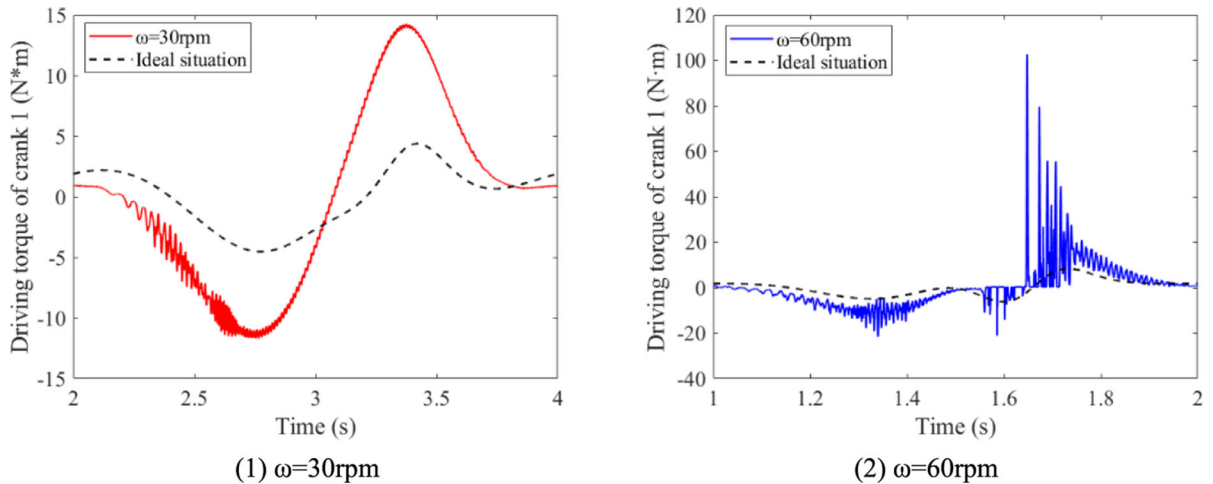


Fig. 33 Driving torque

response under different driving speeds is shown in Table 5. The center trajectory diagrams show that the smaller the driving speed, the closer the trajectory of shaft and trajectory of the slider are to the ideal curve, and the smaller the influence of clearance pairs and flexibility of component on dynamic response.

3.5.2 Analysis of nonlinear characteristics

Phase diagram and Poincaré map shown in Figs. 36, 37 compare and analyze the effect of driving speeds on chaotic characteristics. With the increase of the driving speed, the area of phase diagram at revolute clearance and translational clearance expands and the

degree of confusion increases. With the increase of the driving speed, the area of point of Poincaré mapping of the rotating clearance pair in the X and Y directions and the point of Poincaré mapping of translational clearance pair in the X direction expand and the degree of dispersion strengthens. However, the point of Poincaré mapping of translational clearance pair in the Y direction has always been a point. It can be seen that the driving speed has little effect on motion state of slider in the Y direction. As shown in the bifurcation diagrams of the rotating clearance pair in the X and Y directions and the bifurcation diagram of the translational clearance pair in the X direction (Figs. 38a, b and c), with the increase of the driving speed, the chaos

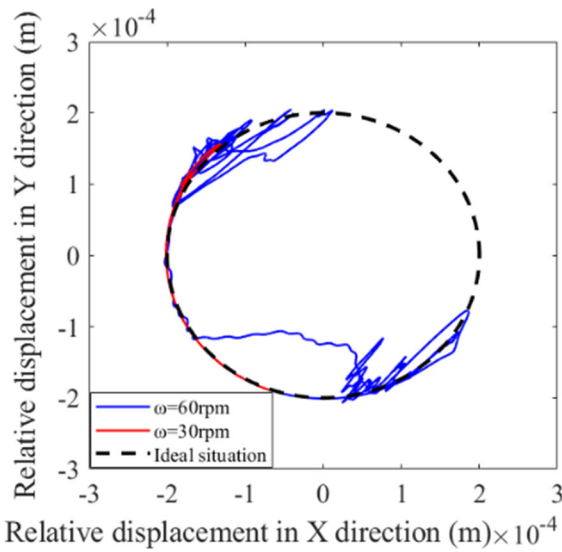


Fig. 34 Trajectory of revolute clearance joint

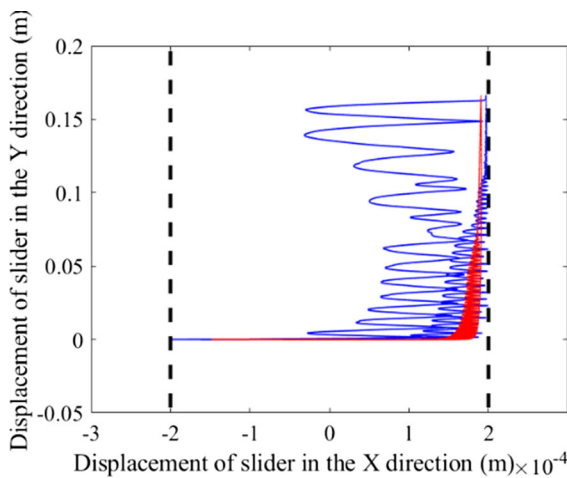


Fig. 35 Trajectory of translational clearance joint

becomes more and more serious and the mechanism becomes more unstable. The bifurcation diagram of translational clearance pair in the Y direction has not changed and has been in the state of periodic motion.

3.6 Virtual simulation verification

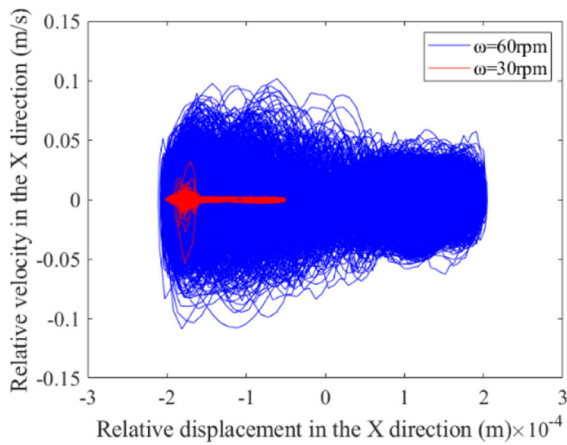
The virtual simulation model of six-bar mechanism is established through ADAMS, considering the revolute clearance pair A and translational clearance pair B, and the component flexibility of components 2, 3 and 4. The clearance value of clearance pair and driving speed of crank are 0.5 mm and 150 rpm, respectively. The dynamic response comparison diagrams corresponding to MATLAB and ADAMS are shown in Figs. 39, 40, 41, 42. Through the comparative analysis of MATLAB curve and ADAMS curve, the displacement curve and speed curve of the mechanism almost coincide, but the acceleration and torque curve deviate to a certain extent, which have basically the same trend. The main reason is that the modeling methods and solving methods of the two software are different, which leads to the deviation of the dynamic response. Therefore, it can be generally considered that theoretical model is correct.

3.7 Test verification

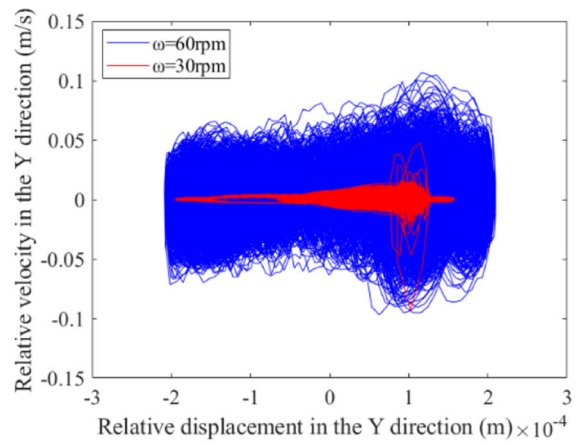
In order to verify the correctness of theoretical model, test platform as shown in Fig. 43 is built. The motion characteristic of the slider of the test platform are measured by acceleration sensor, acceleration sensor is shown in Fig. 44. Data acquisition card shown in Fig. 45 plays a role of connecting signal detection

Table 5 The maximum peak value of dynamic response under different driving speeds

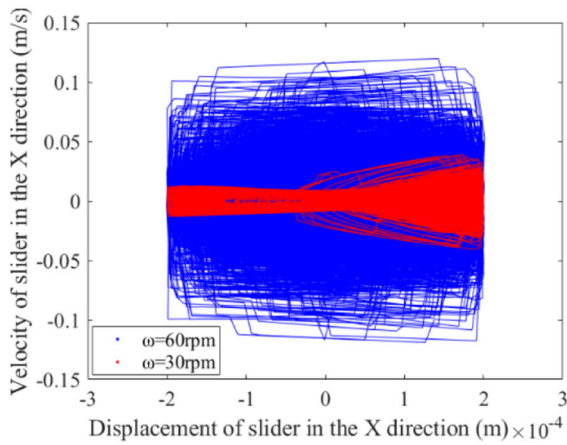
	Driving speed = 30 rpm	Driving speed = 60 rpm
Displacement	0.1667 m	0.1674 m
Velocity	-0.4412 m/s	-0.9177 m/s
Acceleration	5.682 m/s ²	53.46 m/s ²
Torque	14.24 N·m	102.6 N·m



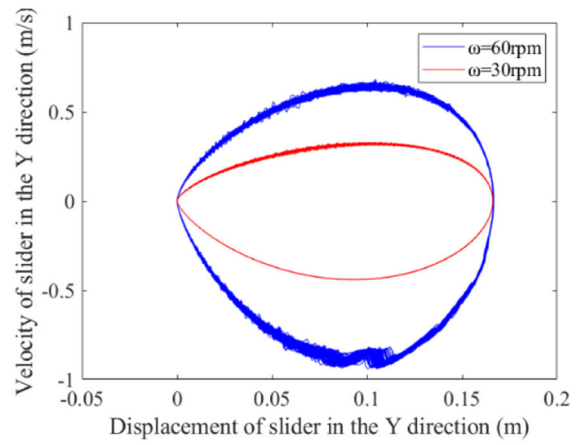
(1) Revolute clearance in X direction



(2) Revolute clearance in Y direction

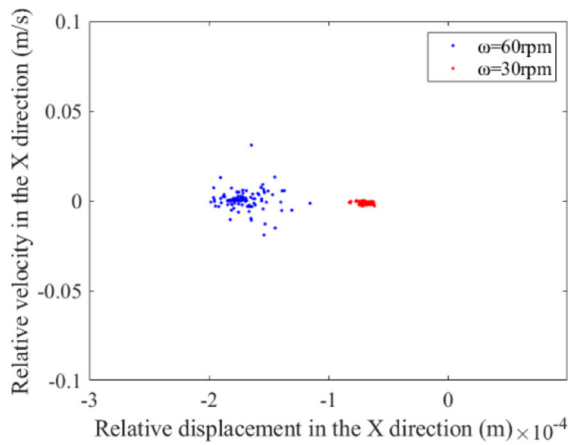


(3) Translational clearance in X direction

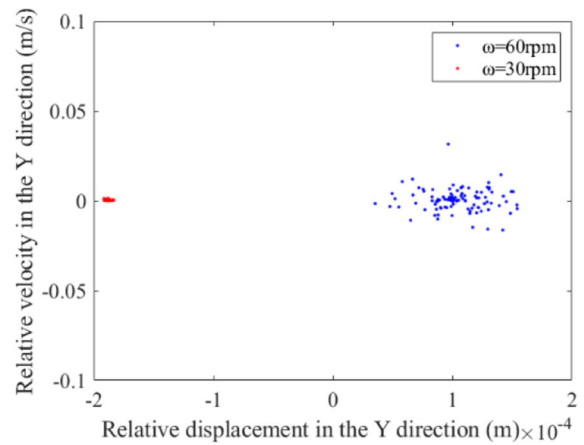


(4) Translational clearance in Y direction

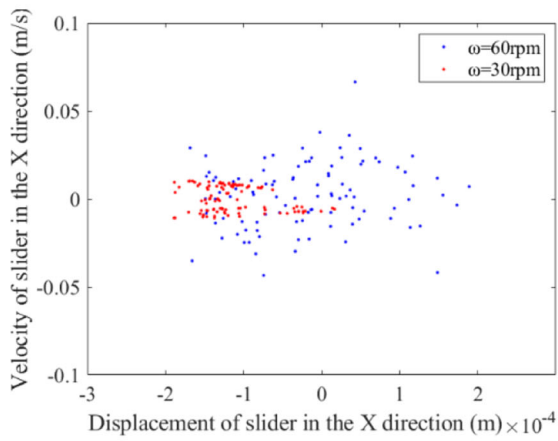
Fig. 36 Phase diagram



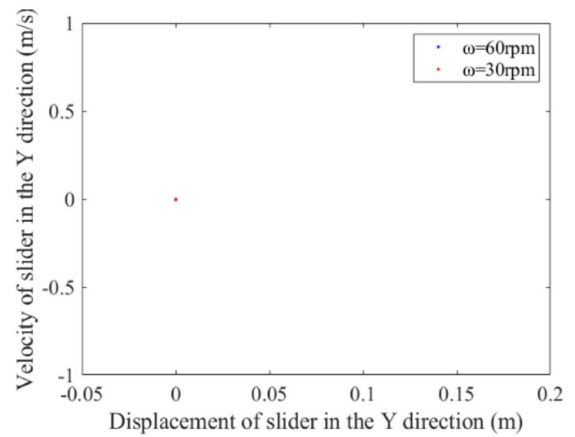
(1) Revolute clearance in X direction



(2) Revolute clearance in Y direction



(3) Translational clearance in X direction



(4) Translational clearance in Y direction

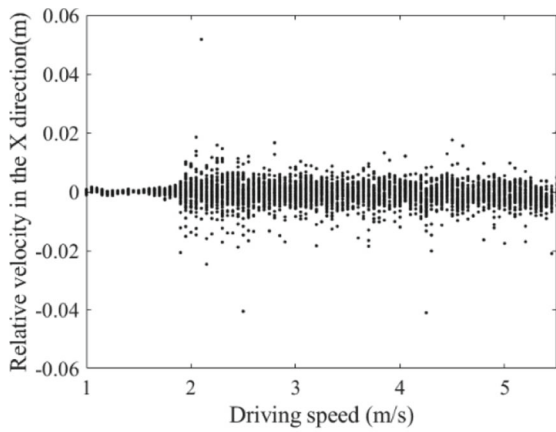
Fig. 37 Poincaré map

element and computer, and it is the key component to ensure the working performance of the whole system.

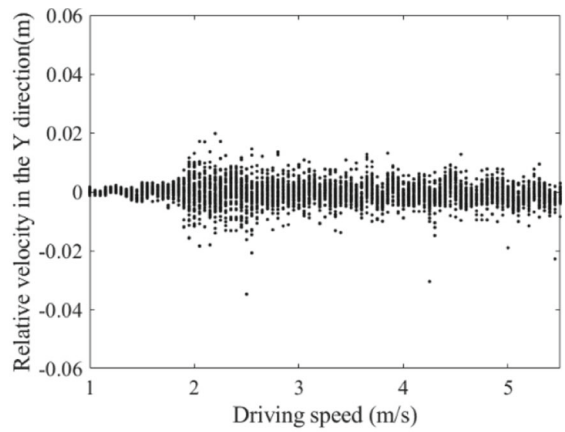
The clearance size of revolute pair A and the translational pair B are both set 0.3 mm, as shown in Figs. 46, 47. The diameter of ideal pin is 15 mm. Length of the cross section of ideal slider is $50 \times 100\text{mm}^2$. The driving speed is set 60 rpm.

When the mechanism has revolute clearance A and translational clearance B, the comparison between theoretical results and experimental results is shown in Fig. 48.

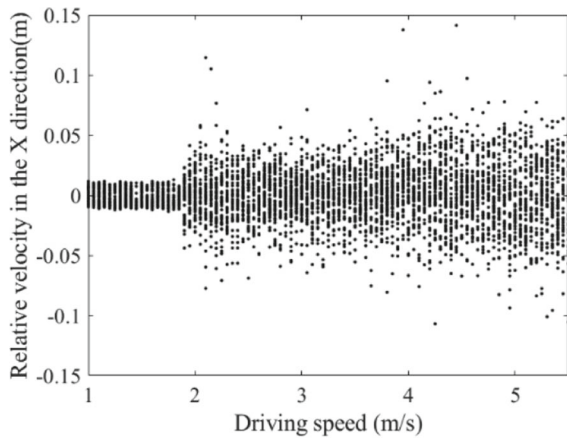
From the comparison between theoretical results and experimental results, the trend of theoretical result and experimental result is basically consistent, but



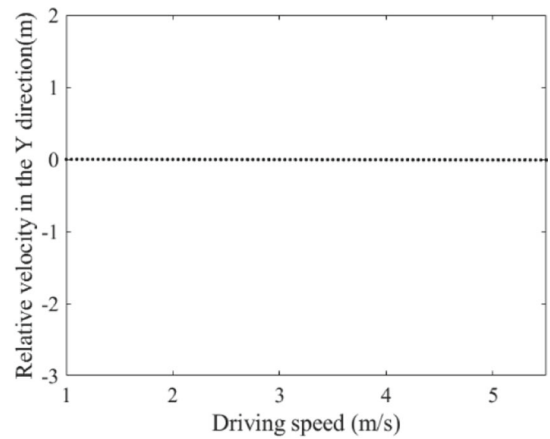
(1) Revolute clearance in X direction



(2) Revolute clearance in Y direction



(3) Translational clearance in X direction



(4) Translational clearance in Y direction

Fig. 38 Bifurcation diagram varying with driving velocity

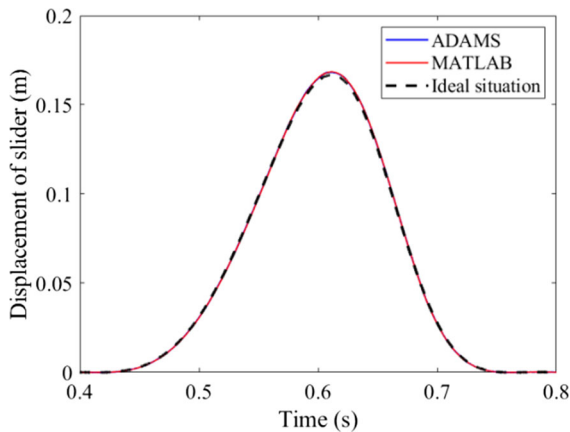


Fig. 39 Displacement

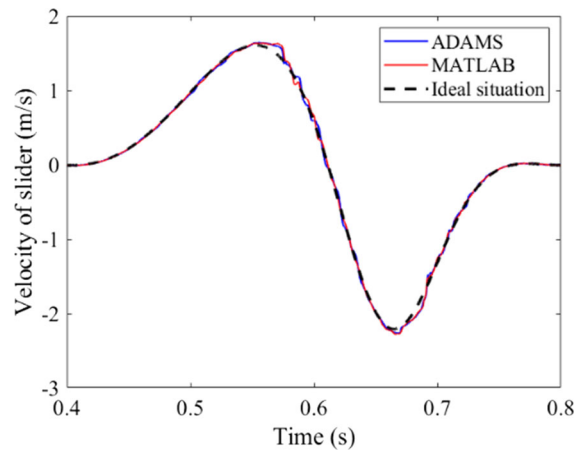


Fig. 40 Velocity

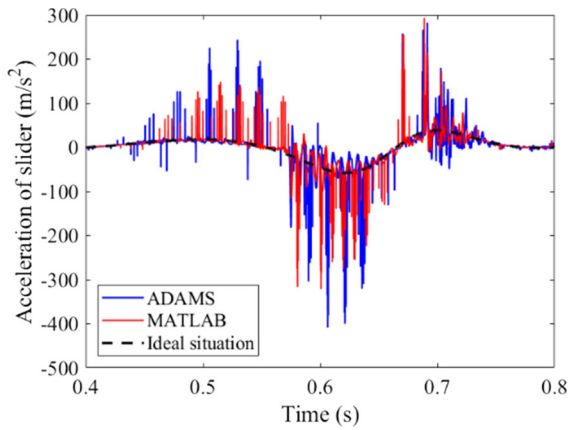


Fig. 41 Acceleration

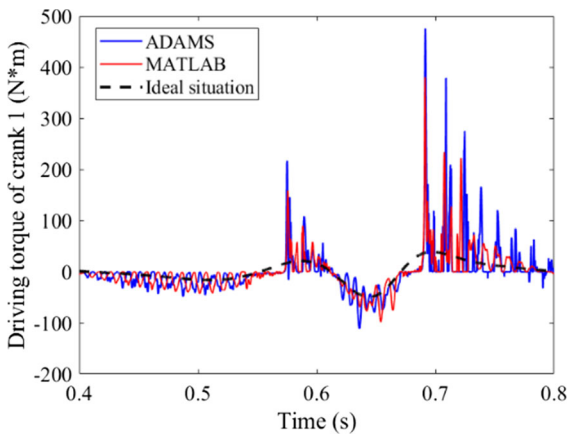


Fig. 42 Driving torque

there are certain differences in the vibration frequency and peak value. The main reason is that friction between components and the lubrication between slider and guide rail will lead to errors. And then, the correctness of the theoretical model can be basically verified.

4 Conclusion

Based on the dynamic of flexible multi-body system, considering the coupling effects of revolute clearance, translational clearance and elastic deformation of components, an accurate dynamic model of multi-body linkage mechanism is proposed.

- (1) Based on ANCF and RPCM, a six-link accurate



Fig. 43 Test platform



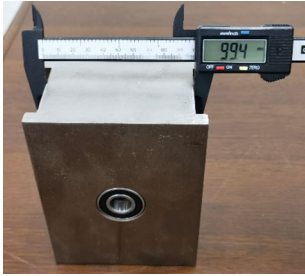
Figs. 44 Acceleration sensor



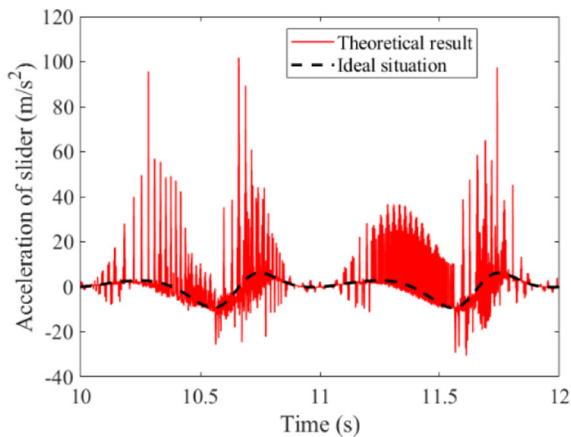
Figs. 45 Data acquisition card



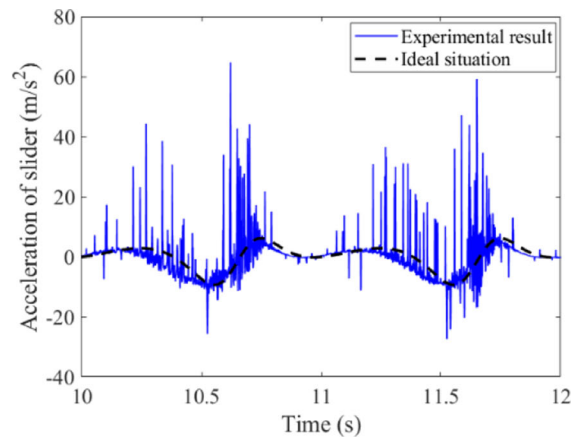
Figs. 46 Shaft(clearance = 0.3 mm)



Figs. 47 Slider(clearance = 0.3 mm)



(1) Theoretical result



(2) Experimental result

Fig. 48 The comparison between the theoretical result and the experimental result

dynamic model considering the coupling effects of revolute clearance, translational clearance and elastic deformation of components is established by using LMD.

- (2) Dynamic response and chaos identification of rigid-flexible coupling mechanism with revolute clearance and translational clearance are researched. It is found that the accuracy and stability of the mechanism are affected by the coupling effects of revolute clearance pair, translational clearance pair and elastic deformation of components. The chaotic state is determined qualitatively and quantitatively by phase diagram, Poincaré map and LLE. It is found that there is chaos in the mechanism.
- (3) Influences of different clearance values and driving speeds on nonlinear dynamic behavior of rigid-flexible coupling mechanism with revolute clearance and translational clearance are analyzed. With the increase of clearance value

and driving speed, the stability and accuracy of mechanism decrease, the chaos of the revolute clearance in the X and Y direction and translational clearance in the X direction increases gradually, and the chaos of translational clearance in the Y direction has been in periodic motion.

- (4) The dynamic modeling method is compared and verified by ADAMS. The correctness of theoretical model is further verified by building an experimental platform.

Funding This research is supported by National Natural Science Foundation of China (Grant no. 61703243) and National Natural Science Foundation of China (Grant no. 51774193).

Data availability The data used to support the results of this research are included in this paper.

Declarations

Conflicts of interest Authors declare that they have no conflict of interest.

References

- Jia, Y., Chen, X.: Application of a new conformal contact force model to nonlinear dynamic behavior analysis of parallel robot with spherical clearance joints. *Nonlinear. Dyn.* **108**(3), 2161–2191 (2022)
- Filipe, M., Paulo, F., Pimenta, C.J.C., et al.: Modeling and analysis of friction including rolling effects in multibody dynamics: a review. *Multibody. Sys.Dyn.* **45**(2), 223–244 (2019)
- Guo, J., He, P., Liu, Z., et al.: Investigation of an improved planar revolute clearance joint contact model with rough surface. *Tribol. Int.* **134**, 385–393 (2019)
- Wang, X.: A method for dynamic modeling and simulation of the translational joint with clearance and LuGre friction. *Mod. Phys. Lett. B* **32**, 34–36 (2018)
- Varedi-Koulaei, S.M., Daniali, H.M., Farajtabar, M., et al.: Reducing the undesirable effects of joints clearance on the behavior of the planar 3-RRR parallel manipulators. *Nonlinear. Dyn.* **86**(2), 1007–1022 (2016)
- Li, Y., Wang, C., Huang, W.: Rigid-flexible-thermal analysis of planar composite solar array with clearance joint considering torsional spring, latch mechanism and attitude controller. *Nonlinear. Dyn.* **96**, 2031–2053 (2019)
- Hou, Y., Deng, Y., Zeng, D.: Dynamic modelling and properties analysis of 3RSR parallel mechanism considering spherical joint clearance and wear. *J. Cent. South. Univers.* **28**(3), 712–727 (2021)
- Wang, G., Qi, Z., Wang, J.: A differential approach for modeling revolute clearance joints in planar rigid multibody systems. *Multibody. Syst. Dyn.* **39**(4), 311–335 (2017)
- Zhu, C., Zhao, Z.: Research on influence of joint clearance on precision of 3-TPT parallel robot. *Mech. Sci.* **10**(1), 287–298 (2019)
- Koshy, C.S., Flores, P., Lankarani, H.M.: Study of the effect of contact force model on the dynamic response of mechanical systems with dry clearance joints: computational and experimental approaches. *Nonlinear. Dyn.* **73**, 325–338 (2013)
- Tian, Q., Flore, P., Lankarani, H.M.: A comprehensive survey of the analytical, numerical and experimental methodologies for dynamics of multibody mechanical systems with clearance or imperfect joints. *Mech. Mach. Theory* **122**, 1–57 (2018)
- Akhadkar, N., Acary, V., Brogliato, B.: Multibody systems with 3D revolute joints with clearances: an industrial case study with an experimental validation. *Multibody. Sys.Dyn.* **42**, 249–282 (2017)
- Shuai, J., Xiulong, C.: Reducing undesirable effects of clearances on dynamic and wear of planar multi-link mechanism. *Nonlinear. Dyn.* **100**, 1173–1201 (2020)
- Chen, X., Wang, T., Jiang, S.: Study on dynamic behavior of planar multibody system with multiple lubrication clearance joints. *Eur. J. Mech. A. Solids.* **91**, 104404 (2022)
- Erkaya, S.: Investigation of joint clearance effects on actuator power consumption in mechanical systems. *Measurement* **134**, 400–411 (2019)
- Liang, D., Song, Y., Sun, T., et al.: Rigid-flexible coupling dynamic modeling and investigation of a redundantly actuated parallel manipulator with multiple actuation modes. *J. Sound. Vib.* **403**, 129–151 (2017)
- Chen, X., Gao, S.: Dynamic accuracy reliability modeling and analysis of planar multi-link mechanism with revolute clearances. *Eur. J. Mech. A. Solids.* **90**, 104317 (2021)
- Hou, Y., Wang, Y., Jing, G., et al.: Chaos phenomenon and stability analysis of RU-RPR parallel mechanism with clearance and friction. *Adv. Mech. Eng.* **10**(1), 168781401774625 (2018)
- Tan, H., Hu, Y., Li, L.: Effect of friction on the dynamic analysis of slider-crank mechanism with clearance joint. *Int. J. Non-Linear Mech.* **115**, 20–40 (2019)
- Chen, X., Jiang, S., Wang, T.: Dynamic modeling and analysis of multi-link mechanism considering lubrication clearance and flexible components. *Nonlinear. Dyn.* **107**(4), 3365–3383 (2022)
- Chen, Z., Qian, L., Chen, G., et al.: Dynamics of luffing motion of a hydraulically driven shell manipulator with revolute clearance joints. *Def. Technol.* **18**, 689–708 (2021)
- Li, B., Wang, M.S., Gantes, C.J., et al.: Modeling and simulation for wear prediction in planar mechanical systems

- with multiple clearance joints. *Nonlinear. Dyn.* **108**(2), 887–910 (2022)
23. Chen, X., Jiang, S.: Dynamic response and chaos in planar multi-link mechanism considering revolute clearances. *Arch. Appl. Mech.* **90**, 1919–1941 (2020)
 24. Marques, F., Isaac, F., Dourado, N., et al.: An enhanced formulation to model spatial revolute joints with radial and axial clearances. *Mech. Mach. Theory.* **116**, 123–144 (2017)
 25. Wan, Q., Liu, G., Shi, H., et al.: Analysis of dynamic characteristics for momentum wheel assembly with joint clearance. *Adv. Mech. Eng.* **10**(12), 1–12 (2018)
 26. Li, S.H., Han, X.Y., Wang, J.Q., et al.: Contact Model of Revolute Joint with Clearance Based on Fractal Theory. *Chin. J. Mech. Eng.* **31**, 109 (2018)
 27. Bai, Z., Zhao, J.: A Study on dynamic characteristics of satellite antenna system considering 3D revolute clearance joint. *Int. J. Aeronaut. Eng.* **2020**(4), 1–15 (2020)
 28. Alshaer, B.J., Nagarajan, H., Beheshti, H.K., et al.: Dynamics of a multibody mechanical system with lubricated long journal bearings. *J. Mech. Des.* **127**(3), 493–498 (2005)
 29. Xu, L.X., Han, Y.C., Dong, Q.B., et al.: An approach for modelling a clearance revolute joint with a constantly updating wear profile in a multibody system: simulation and experiment. *Multibody. Sys.Dyn.* **45**, 457–478 (2019)
 30. Zhang, F., Yuan, Z.: The study of coupling dynamics modeling and characteristic analysis for flexible robots with nonlinear and frictional joints. *Arab. J. Sci. Eng.* **12**, 1–7 (2022)
 31. Zheng, E., Wang, T., Guo, J., et al.: Dynamic modeling and error analysis of planar flexible multilink mechanism with clearance and spindle-bearing structure. *Mech. Mach. Theory* **131**, 234–260 (2019)
 32. Chen, X., Jiang, S., Wang, S., et al.: Dynamics analysis of planar multi-DOF mechanism with multiple revolute clearances and chaos identification of revolute clearance joints. *Multibody. Sys. Dyn.* **47**, 317–345 (2018)
 33. Li, Y., Li, M., Liu, Y., et al.: Parameter optimization for torsion spring of deployable solar array system with multiple clearance joints considering rigid–flexible coupling dynamics. *Chin. J. Aeronaut.* **35**, 509–524 (2021)
 34. Wang, Q., Tian, Q., Hu, H.: Dynamic simulation of frictional contacts of thin beams during large overall motions via absolute nodal coordinate formulation. *Nonlinear. Dyn.* **77**(4), 1411–1425 (2014)
 35. Yaqubi, S., Dardel, M., Daniali, H.M.: Nonlinear dynamics and control of crank-slider mechanism with link flexibility and joint clearance. *Proc. Inst. Mech. Eng. Part. C. J. Mech. Eng. Sci.* **230**(5), 737–755 (2015)
 36. Shuai, J., Xiulong, C.: Test study and nonlinear dynamic analysis of planar multi-link mechanism with compound clearances. *Eur. J. Mech. A. Solids.* **88**, 104260 (2021)
 37. Meng, F., Wu, S., Fan, Z., et al.: Modeling and simulation of flexible transmission mechanism with multiclearance joints for ultrahigh voltage circuit breakers. *Shock. Vib.* **2015**, 392328 (2015)
 38. Pi, T., Zhang, Y.: Modeling and simulation of revolute clearance joint with friction using the NURBS-based isogeometric analysis[J]. *Nonlinear Dyn.* **95**, 195–215 (2018)
 39. Jiang, G.Q., Yang, X.D., Zhang, W., et al.: The modeling and dynamic analysis of two jointed beams with clearance. *Appl. Math. Model.* **74**, 528–539 (2019)
 40. Chen, Y., Wu, X., Wu, K., et al.: An experimental and analytical study on dynamic behaviors of high-precision mechanism including revolute clearance joints. *J. Braz. Soc. Mech. Sci. Eng.* **44**(4), 120 (2022)
 41. Xiang, W., Yan, S.: Dynamic analysis of space robot manipulator considering clearance joint and parameter uncertainty: Modeling, analysis and quantification. *Acta. Astronaut.* **169**, 158–169 (2020)
 42. Li, B., Wang, S.M., Gantes, C.J., et al.: Nonlinear dynamic characteristics and control of planar linear array deployable structures consisting of scissor-like elements with revolute clearance joint. *Adv. Struct. Eng.* **24**(1), 136943322097172 (2020)
 43. Chen, Z., Qian, M., Sun, F., et al.: A quantitative analysis method for contact force of mechanism with a clearance joint based on entropy weight and its application in a six-bar mechanism. *Chin. Phys. B* **31**(4), 044501 (2022)
 44. Chen, Z., Qian, L.: Nonlinear dynamic characteristics analysis of planar flexible rotating beams with clearance joint. *J. Braz. Soc. Mech. Sci. Eng.* **42**(6), 333 (2020)
 45. Li, Y., Yang, Y., Li, M., et al.: Dynamics analysis and wear prediction of rigid-flexible coupling deployable solar array system with clearance joints considering solid lubrication. *Mech. Syst. Signal. Process.* **162**(7–8), 108059 (2022)
 46. Stoenescu, E.D., Dan, B.M.: Dynamic analysis of a planar rigid-link mechanism with rotating slider joint and clearance. *J. Sound. Vib.* **266**(2), 394–404 (2003)
 47. Wu, X., Sun, Y., Wang, Y., et al.: Dynamic analysis of the double crank mechanism with a 3D translational clearance joint employing a variable stiffness contact force model. *Nonlinear. Dyn.* **99**, 1937–1958 (2019)
 48. Flores, P., Leine, R., Glocker, C.: Modeling and analysis of planar rigid multibody systems with translational clearance joints based on the non-smooth dynamics approach. *Multibody. Sys.Dyn.* **23**(2), 165–190 (2010)
 49. Qian, M., Qin, Z., Yan, S., et al.: A comprehensive method for the contact detection of a translational clearance joint and dynamic response after its application in a crank-slider mechanism. *Mech. Mach. Theory* **145**, 103717 (2020)
 50. Flores, P., Ambrósio, J., Claro, J.C.P., et al.: Translational joints with clearance in rigid multibody systems. *J. Comput. Nonlinear. Dyn.* **3**(1), 112–113 (2008)
 51. Chen, X., Jiang, S., Deng, Y.: Dynamic responses of planar multilink mechanism considering mixed clearances. *Shock. Vib.* **2020**, 8725845 (2020)
 52. Wang, T., Chen, G., Ma, F., et al.: Dynamic analysis of multibody systems with mixed clearance. *J. Vib. Shock.* **35**(9), 178–183 (2016)
 53. Wu, X., Sun, Y., Wang, Y., et al.: Correlation dimension and bifurcation analysis for the planar slider-crank mechanism with multiple clearance joints. *Multibody. Sys.Dyn.* **52**, 95–116 (2021)
 54. Tian, Q., Zhang, Y., Chen, L., et al.: Dynamics of spatial flexible multibody systems with clearance and lubricated spherical joints. *Comput. Struct.* **87**(13–14), 913–929 (2009)
 55. Tian, Q., Liu, C., Machado, M., et al.: A new model for dry and lubricated cylindrical joints with clearance in spatial

- flexible multibody systems. *Nonlinear. Dyn.* **64**(1–2), 25–47 (2011)
56. Baumgarte, J.: Stabilization of constraints and integrals of motion in dynamical systems. *Comput. Methods. Appl. Mech. Eng.* **1**(1), 1–16 (1972)
57. Jiang, S., Chen, X.: Test study and nonlinear dynamic analysis of planar multi-link mechanism with compound clearances. *Eur. J. Mech. A. Solids.* **88**(2), 104260 (2021)

Publisher's Note Springer Nature remains neutral with regard to jurisdictional claims in published maps and institutional affiliations.

Springer Nature or its licensor (e.g. a society or other partner) holds exclusive rights to this article under a publishing agreement with the author(s) or other rightsholder(s); author self-archiving of the accepted manuscript version of this article is solely governed by the terms of such publishing agreement and applicable law.